# Seasonal variability of nutrient concentrations in the Mediterranean Sea: Contribution of Bio-Argo floats

Orens Pasqueron de Fommervault, Fabrizio d'Ortenzio, Antoine Mangin, Romain Serra, Christophe Migon, Hervé Claustre, Héloïse Lavigne, Maurizio Ribera d'Alcalà, Louis Prieur, Vincent Taillandier, et al.

AGU PUBLICATIONS

JGR

Journal of Geophysical Research: Oceans

RESEARCH ARTICLE

10.1002/2015JC011103

**Key Points:**

- Five profiling floats equipped with nitrate sensors were deployed in the Mediterranean Sea
- Annual cycles of nutrient concentrations depicted with an unprecedented temporal resolution
- Major contribution of high-frequency processes highlighted

**Supporting Information:**

- Supporting Information S1

**Correspondence to:**
O. P. de Fommervault,
orens.de-fommervault@obs-vlfr.fr

**Citation:**
Pasqueron de Fommervault, O. et al. (2015), Seasonal variability of nutrient concentrations in the Mediterranean Sea: Contribution of Bio-Argo floats, *J. Geophys. Res. Oceans*, *120*, doi:10.1002/2015JC011103.

Received 6 JUL 2015
Accepted 13 NOV 2015
Accepted article online 19 NOV 2015



# Seasonal variability of nutrient concentrations in the Mediterranean Sea: Contribution of Bio-Argo floats

**Orens Pasqueron de Fommervault[1,2,3], Fabrizio D'Ortenzio[1,2], Antoine Mangin[3], Romain Serra[3], Christophe Migon[1,2], Hervé Claustre[1,2], Héloïse Lavigne[4], Maurizio Ribera d'Alcalà[5], Louis Prieur[1,2], Vincent Taillandier[1,2], Catherine Schmechtig[1,2], Antoine Poteau[1,2], Edouard Leymarie[1,2], Aurélie Dufour[1,2], Florent Besson[1,2], and Grigor Obolensky[1,2]**

[1]Sorbonne Universités, UPMC Université Paris 06, UMR 7093, LOV, Observatoire océanologique, Villefranche-sur-mer, France, [2]CNRS, UMR 7093, LOV, Observatoire océanologique, Villefranche-sur-mer, France, [3]ACRI-ST, Biot, France, [4]Istituto Nazionale di Oceanografia e di Geofisica Sperimentale, Trieste, Italy, [5]Stazione Zoologica Anton Dohrn, Naples, Italy

**Abstract** In 2013, as part of the French NAOS (Novel Argo Oceanic observing System) program, five profiling floats equipped with nitrate sensors (SUNA-V2) together with CTD and bio-optical sensors were deployed in the Mediterranean Sea. At present day, more than 500 profiles of physical and biological parameters were acquired, and significantly increased the number of available nitrate data in the Mediterranean Sea. Results obtained from floats confirm the general view of the basin, and the well-known west-to-east gradient of oligotrophy. At seasonal scale, the north western Mediterranean displays a clear temperate pattern sustained by both deep winter mixed layer and shallow nitracline. The other sampled areas follow a subtropical regime (nitracline depth and mixed layer depth are generally decoupled). Float data also permit to highlight the major contribution of high-frequency processes in controlling the nitrate supply during winter in the north western Mediterranean Sea and in altering the nitrate stock in subsurface in the eastern basin.

## 1. Introduction

The Mediterranean Sea (Med), which extends from 30°N to 45°N, is an elongated semienclosed basin, geographically positioned in the transition zone between temperate and subtropical environments. It is divided into two (western and eastern) subbasins, linked via the shallow (~500 m-depth) Sicilian strait. Overall, according to the definition given by *Longhurst et al.* [1995], the Med is considered an oligotrophic province: it is a low nutrient concentration basin, and one of the largest nutrient-depleted areas in the world [*Siokou-Frangou et al.*, 2010; *Sverdrup et al.*, 1942]. Nutrient molar ratios in the basin display anomalous values, compared to those of other oceanic regions [see *Ribera d'Alcalà et al.*, 2003 for a review].

Recent studies [e.g., *D'Ortenzio and Ribera d'Alcalà*, 2009; *Lazzari et al.*, 2012; *Siokou-Frangou et al.*, 2010; *Pujo-Pay et al.*, 2011] have also evidenced the coexistence of different biogeochemical regimes. At climatological scale, a subtropical-like regime (characterized by very low biomass values and by a smoothed seasonality of physical dynamics) dominates almost the entire Med, while a temperate-like regime (with high value of spring biomass) is found in some specific areas (i.e., in the north western Med, the Southern Adriatic Sea, and the Rhodes gyre area) [*Bosc et al.*, 2004; *D'Ortenzio and Ribera d'Alcalà*, 2009; *Gačić et al.*, 2002; *Ignatiades et al.*, 2009; *Lavigne et al.*, 2013].

The general nutrient depletion of the basin is consensual, and for the most related to the antiestuarine circulation of the Med [*Durrieu de Madron et al.*, 2011]. The few nutrients available in the Atlantic surface inflow entering the Mediterranean Sea are consumed along the way to the eastern basin and exported to intermediate and deep water [*Crise et al.*, 1999; *Lazzari et al.*, 2012]. This results in a negative nutrient budget at Gibraltar [*Coste et al.*, 1988; *Crispi et al.*, 2001] and in a west-to-east gradient of oligotrophy [*Manca et al.*, 2004; *Moutin and Prieur*, 2012; *Pujo-Pay et al.*, 2011]. Moreover, external sources (mainly atmospheric inputs) and organic forms are considered to be relevant to modify the available stock [*Bartoli et al.*, 2005; *Violaki et al.*, 2015]. The coexistence of temperate-like and subtropical-

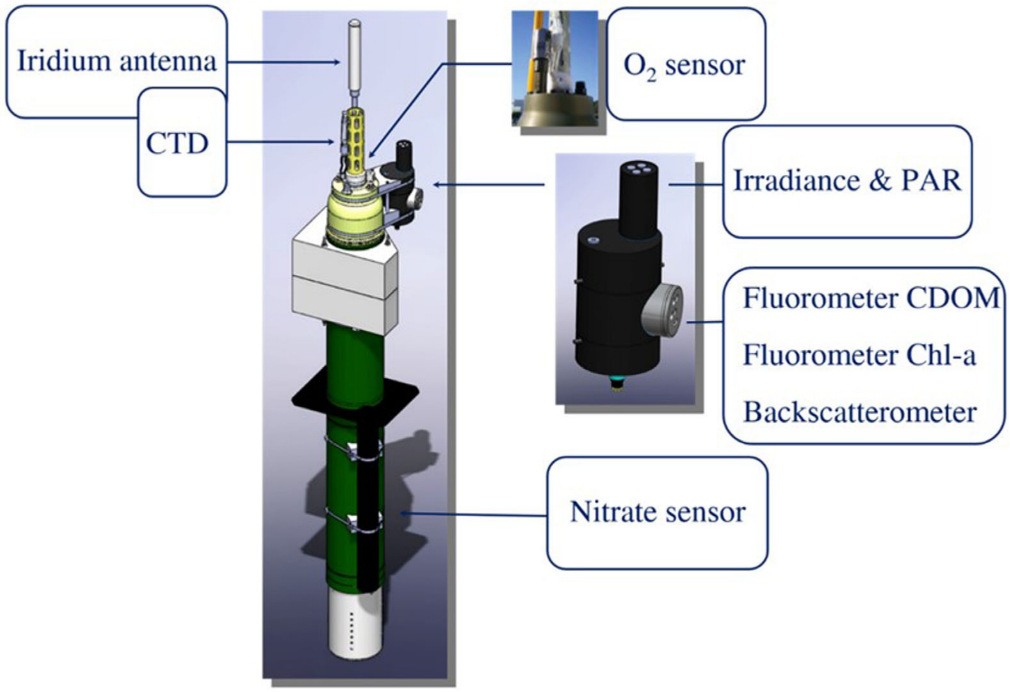


**Figure 1.** Schematic representation of a PROVBIO-V2 float equipped with bio-optical and nitrate sensors (SUNA V2).

like is generally related to the geographical variability of the winter mixed layer depth (MLD) that induces or not the refueling of nutrients to the surface layer [*D'Ortenzio et al*., 2014; *Gačić et al*., 2002; *Lavigne et al*., 2013].

Superimposed on this general low nutrient picture, several sporadic mechanisms, such as local mesoscale activity, may induce nutrient refueling to surface layers and then favor phytoplankton growth [*Jenkins et al*., 2008; *Krom et al*., 1992; *Ledwell et al*., 2008]. In the Med, the presence of such structures was clearly evidenced from remote sensing [*Hamad et al*., 2006; *Larnicol et al*., 1995; *Millot*, 1991; *Robinson et al*., 1991; *Mkhinini et al*., 2014]. Nevertheless, characterized by short duration and sparse geographical occurrence, these structures are hardly detectable from in situ measurements, and their contributions to biogeochemical budgets are only obtained by modeling [*Crise et al*., 1999, 1998]. At basin scale, and except very few areas (where long-term sampling stations exist) [*Marty et al*., 2002], even seasonal/interannual variability is often poorly characterized, at least for the biogeochemical compartments [*Pasqueron de Fommervault et al*., 2015a]. The main cause of this lack of knowledge is the scarcity of field data (notably when meteorological conditions are bad), which is particularly critical regarding nutrient concentrations. This prevents the accurate description of many processes often occurring at scales that are too small to be observable with usual sampling approaches.

Recently, the development of automatized platforms (gliders, buoys, profiling floats, etc.) allowed the emergence of high-frequency annual and multiannual time series, for physical [*Bosse et al*., 2015; *D'Ortenzio et al*., 2014; *Johnson et al*., 2013; *Ruiz et al*., 2012; *Smith et al*., 2008], biological [*Boss et al*., 2008; *Johnson et al*., 2007; *Niewiadomska et al*., 2008; *Xing et al*., 2011], and chemical observations [*Johnson et al*., 2010]. In the Med (more specifically in the north western Med), the first use of profiling floats with nitrate sensors was successful and demonstrated the great potentialities of the approach, even in the conditions as those of the basin (i.e., at the limits of the accuracy of the automatic sensors) [see *D'Ortenzio et al*., 2014]. Following this first attempt, and with the aim to sample a larger area, 12 profiling floats embarking bio-optical sensors together with CTD (hereafter Bio-Argo [*Leymarie et al*., 2013], see Figure 1) were deployed in the Med over the period April–July 2013, as part of the French NAOS program (http://www.naos-equipex.fr/). Five of them were equipped with nitrate sensors (SUNA-V2), and they were deployed in the north western Mediterranean basin (NW Med), the Tyrrhenian Sea (TYR), the Ionian Sea (ION), and the Levantine

Sea (LEV), with the objective to sample contrasted trophic regimes and to characterize the west-to-east gradient of the basin.

In this paper, we focus on chemical data, which are restricted to nitrate concentrations (hereinafter referred to as [$NO_3$]) since the autonomous measurement of other elements from profiling floats is not yet possible (although phosphate is generally considered the limiting factor in the Med) [*Krom et al*., 2010]. For the first time in the Med, we present high-frequency [$NO_3$] time series, using the NAOS Bio-Argo floats, in four different areas. Considering that [$NO_3$] floats profiles derive from an optical measurement, a significant effort was invested to calibrate those profiles. Therefore, in this study, we present data processing and quality control on the nitrate float data specifically developed for the Med. We particularly focus on the Mediterranean annual cycle of [$NO_3$], related to density field, MLD dynamics and satellite (altimetry) data, and on its geographical differences. We discuss in more detail than previous studies, the links between physical dynamics at short time scale and the [$NO_3$] temporal evolution. A comparison with existing historical database permitted also to evidence barely perceptible processes and to evaluate the role of interannual variability. Last, the response of phytoplankton to [$NO_3$] vertical distribution was investigated.

## 2. Data

### 2.1. AVISO Sea Level Anomaly

For the analysis of the large and mesoscale physical conditions, altimetry-derived maps of Sea Level Anomaly (SLA) produced by Ssalto/Duacs and distributed by AVISO, with support from CNES (http://www.aviso.altimetry.fr/duacs) were used. Data are gridded and provided in Delayed Time with a spatial resolution of 1/8°. Note that the horizontal resolution is of the order of the internal deformation radius in the Med, meaning that only mesoscales structures with a radius larger than ~10–12 km could be identified from this data [*Mkhinini et al*., 2014].

### 2.2. Nitrate Historical Database

The historical database consists of 5318 nitrate concentration profiles assembled for the whole Med over the 1961–2010 period. Data were obtained from the MEDAR-MEDATLAS [*Maillard et al*., 2005], MATER [*Maillard et al*., 2002], and SESAME (http://www.sesame-ip.eu) programs as well as from specific cruises, and compiled by *Lavezza et al*. [2011]. The resulting data set is an inventory of several cruises, operators, methods, etc. and reveals a strong heterogeneity. The quality control procedure described by *Lavigne et al*. [2013] was applied to remove spikes, outliers, and incomplete profiles (less than five valid data points). To our knowledge, the data set is the most complete for the Med, but in spite of the high number of available profiles (2564 after the quality control procedure), large areas of the basin are undersampled and the temporal resolution remains quite low.

Surface nitrate concentrations $[NO_3]_{surf}$ and nitrate concentrations at depth $[NO_3]_{deep}$ were calculated as the mean value in the 0–30 and 900–1100 m-depth layers, respectively. The data set was then split in to four geographic areas along a 4° latitude width transect, supposed to be representative of the bioregions [in the sense of *D'Ortenzio and Ribera d'Alcalà*, 2009] where floats were deployed (i.e., NW Med, TYR, LEV, and ION, see dashed lines in Figure 2).

### 2.3. Floats Database

The float database is composed of five time series obtained by five Bio-Argo floats deployed in the Med and equipped with SUNA sensors (PROVBIO-V2). The PROVBIO-V2 is based on the PROVOR CTS4 profiling float (http://www.nke-instrumentation.fr/). The float is equipped with chlorophyll (Chl) and colored dissolved organic matter fluorometers, optical backscattering coefficient, photosynthetically available radiation sensors, and three wavelength irradiance radiometers. It is additionally equipped with Iridium telemetry, allowing a double way communication and then the capability to modify sampling strategy during the mission. The nitrate sensor was externally clamped to the float suitcase around 1.5 m below the CTD intake (Figure 1).

As an Argo float, Bio-Argo floats spent most of the time at depth (i.e., 1000 m for the Med floats), starting a profile at a given temporal resolution, and transmitting data at the end of the profiling phase (i.e., at surface). Temporal sampling for the Med floats was initially fixed to 5 days, to be increased up to a daily resolution during specific periods (i.e., winter-to-spring transition). As part of the general deployment strategy of

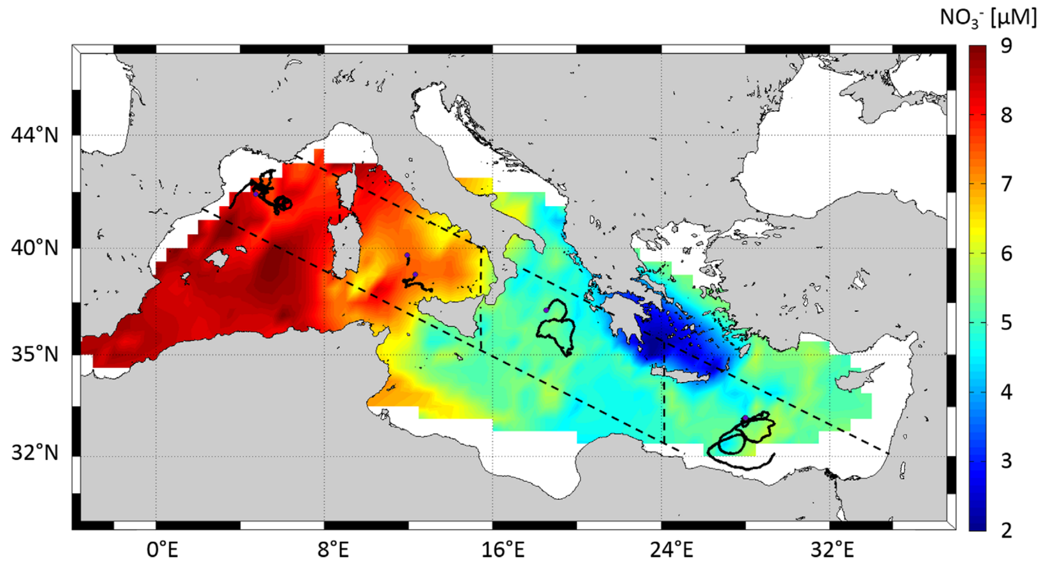


**Figure 2.** Map of deep nitrate concentrations (average values below 800 m depth) in the Med. Data are interpolated using a triangle-based cubic method. Black lines represent float trajectories, and dashed lines limit the four areas considered for seasonal analysis (NW Med, TYR, LEV, and ION).

the NAOS Bio-Argo floats in the Med, which was driven by the existing Med bioregionalization [*D'Ortenzio and Ribera d'Alcalà*, 2009] (see also the NAOS roadmap for the Med, http://goo.gl/kUIVWc), the deployment plan for the $NO_3$ floats was specifically driven by the requirement to cover the west-to-east gradient of decreasing [$NO_3$]. One float (lovbio017b) was deployed in the NW Med on April 2013 and its position was relatively stable during the whole mission for almost a year (145 profiles). In the TYR, the float lovbio042c was deployed in June 2013, although after nine profiles it experienced severe technical issues, and it was recovered and replaced by the lovbio039b in July 2013. However, after 59 profiles, also the lovbio039b failed. The two TYR time series were then assembled and considered as a single series. However, the resulting time series did not complete an annual cycle. The lovbio016c and the lovbio018c were respectively launched in the ION and the LEV in May 2013. At present day (June 2015), they are still operational. An overview of practical information about float missions is given in Table 1, and float trajectories can be viewed in Figure 2.

[$NO_3$] estimations were performed from 0 to 1000 m-depth (about 10 m resolution in the 0–250 m layer, and 30 m in the remaining range). [$NO_3$] estimations (values computed by the SUNA software in real time, see below), as well as raw data (i.e., absorbance spectrum from 217 to 250 nm) were transmitted. Specific calibration and quality control procedures were performed, which are developed in section 3. Overall, floats collected 489 [$NO_3$] profiles over the years 2013–2014, and, compared to the historical database, the resulting database is very homogenous, although limited to a restricted period and to specific areas. Temperature, salinity, and fluorescence profiles were also collected, through a higher vertical resolution. For temperature and salinity, the sampling rate was about 1 m in the 0–100 m layer and 10 m at depth, and for fluorescence it was around 1 m from 0 to 250 m and 5 m below. Argo and Bio-Argo real-time quality control procedures were then applied [*Schmechtig et al.*, 2014; *Wong et al.*, 2014], and fluorescence data were converted into [Chl] according to the protocol of *Lavigne et al.* [2012].

**Table 1.** Overview of Practical Information About Float Mission

| Float | Location | First Profile | Profile Number | Last Profile | Current State |
|---|---|---|---|---|---|
| *Lovbio017b* | NW Med | 9 Apr 2013 | 145 | 4 May 2014 | Dead |
| *Lovbio042c* | TYR | 16 Jun 2013 | 009 | 7 Jul 2013 | Dead |
| *Lovbio039b* | TYR | 23 Jul 2013 | 059 | 27 Mar 2014 | Dead |
| *Lovbio016c* | ION | 26 May 2013 | 130 | 2 Jan 2014 | Operational |
| *Lovbio018c* | LEV | 16 May 2013 | 146 | 21 May 2014 | Operational |

**Table 2.** Calibration Coefficient for Nitrate Concentration Profiles

| Float | *wl* ($m^{-1}$) | Offset ($\mu$mol $L^{-1}$) | Drift ($\mu$mol $L^{-1}$ profil$^{-1}$) |
|---|---|---|---|
| *Lovbio017b* | 208.0 | +0.3 | 0.0104 |
| *Lovbio042c* | 210.0 | −3.9 | 0.0138 |
| *Lovbio039b* | 208.0 | −0.7 | 0.0195 |
| *Lovbio016c* | 209.0 | −0.5 | −0.0140 |
| *Lovbio018c* | 208.5 | −1.1 | 0.0145 |

## 3. Nitrate Sensor Calibration and Quality Control

### 3.1. Nitrate Sensor Calibration

The SUNA sensor has been developed for the direct determination of [$NO_3$], by deconvoluting the measured light absorption at ultraviolet wavelengths with a dedicated algorithm [*D'Ortenzio et al.*, 2012; *Johnson and Coletti*, 2002; *Johnson et al.*, 2010, 2013]. Recently, an improved algorithm (the Temperature Compensated Salinity Subtracted [TCSS]) has been developed to account for the temperature dependence of bromide spectra and its influence on the ultraviolet deconvolution [*Sakamoto et al.*, 2009]. In the Med, the TCSS algorithm required slight modifications, for the most related to the extremely high values of temperature observed and to the requirement to increase accuracy in an environment of very low [$NO_3$]. The observed biases (described further) were detected on the whole float database, and more specifically evidenced, when direct comparisons with available [$NO_3$] profiles obtained by colorimetric measurements were carried out (i.e., at the lovbio017b and lovbio042c deployments). Corrections were then initially determined on the lovbio017b and lovbio042c floats, to be further applied to the whole database.

A bias in [$NO_3$] was observed when temperature was higher than 20°C (see supporting information S1 for an example). The bias, which is related to the specific optical characteristics of each sensor, was corrected by modifying the wavelength offset (*wl*) used in the TCSS algorithm [*Sakamoto et al.*, 2009]. Spikes or aberrant values were also detected on the vertical profiles of [$NO_3$], in particular when layers with strong temperature and salinity gradients were sampled. The distance on the float between the position of the CTD and the SUNA sensors (about 1.5 m) is likely the origin of this error, as temperature and salinity measurements used by the TCSS algorithm were not relative to the water portion sampled by the SUNA. The bias was then corrected by using, in the TCSS algorithm, temperature and salinity values obtained interpolating linearly the CTD profile at the depth of the SUNA. Another error was detected by comparison with climatological values, with a TCSS overestimation up to 60% at 1000 m depth. Although a natural variability was always possible, the lack of any pressure correction terms in the spectral model of the TCSS algorithm was considered the primary source of this error. The pressure effect, again, could be particularly significant (and thus, observable) in the Med, where [$NO_3$]$_{deep}$ concentrations are strongly lower than those measured in other environments [see for example, *Johnson et al.* 2013]. A pressure dependence of bromide spectra was suspected, and an empirical additional correction was applied to the extinction coefficient of seawater (equation (1)):

$$ESW_{(\lambda,Tis,P)} = ESW_{(\lambda,Tis)} \cdot \left(1 - f \cdot \frac{P}{1000}\right) \tag{1}$$

where $ESW_{(\lambda,Tis,P)}$ is the modified extinction coefficient of seawater corrected to in situ pressure, $ESW_{(\lambda,Tis)}$ is the extinction coefficient of seawater given by *Sakamoto et al.* [2009], *P* is the pressure, and *f* the correction factor that corresponds to 2% per 1000 dbar. This latter value was derived considering the lovbio017b and lovbio042c deployment profiles (to impose match with colorimetric values at depth) and also by a dedicated test in the Villefranche-sur-Mer Bay (detailed in supporting information S2).

Finally, the SUNA sensor could be affected by an instrumental drift when long-term missions are performed [see *Johnson et al.*, 2013]. The correction method proposed by *Johnson et al.* [2013] has been here slightly adapted to the specific Med conditions. The long-term drift was initially determined from the slope of a linear regression of [$NO_3$] at depth (average value between 800 and 1000 m depth) versus cycle number. Offsets were then calculated by comparison with climatological values in summer (i.e., when [$NO_3$] is supposed to be exhausted in surface). The calibration coefficients for the whole database are given in Table 2.

### 3.2. Quality Control

For [$NO_3$] profiles, a specific quality control was developed. All the data points acquired in surface, i.e., when the pressure measured by the CTD was negative, were discarded (23 points). A test for spike was then applied using three $[NO_3]$ consecutive measurements. The product ($P_N$) of two consecutive slopes was computed and compared to a threshold values (equation (2)).

$$P_N = \frac{[NO_3]_{P_i} - [NO_3]_{P_{i-1}}}{P_i - P_{i-1}} \cdot \frac{[NO_3]_{P_{i+1}} - [NO_3]_{P_i}}{P_i - P_{i+1}} \tag{2}$$

where $P$ is the pressure, $[NO_3]_{P_i}$ the nitrate measurement being tested as a spike, and $[NO_3]_{P_i-1}$ and $[NO_3]_{P_i+1}$ the values immediately above and below, respectively. $[NO_3]_{P_i}$ was flagged when $P_N$ was lower than $-0.008$ (determined from visual inspection), meaning that a steep inversion of the slope exists (i.e., low $P_N$ value). Data that failed the test were flagged as spikes (i.e., bad data) and removed from the data set. Because spike might be sometimes caused by several points, the test was reiterated until no additional bad data were identified. A total of 583 points were removed, essentially above 100 m depth.

Two diagnostic tests were then applied to check measurement accuracy (Kenneth S. Johnson, personal communication, 2014). In the first one, the absorbance of the in situ spectrum at the first wavelength greater than 240 nm was computed. If this value was higher than 1.1, the data point was discarded. The rationale of the test is that the measured absorbance spectrum is not necessarily dominated by $[NO_3]$ (due, for example, to elevated bisulfide concentration) [*Johnson and Coletti*, 2002; *Ogura and Hanya*, 1966], and the application of the TCSS algorithm concentration, using the 217–240 nm range, may not be correct. In the second diagnostic test, the root-mean-square error of the residuals of the predicted absorbance spectrum from the measured spectrum over the range 217–240 nm is calculated. Data points exhibiting a root-mean-square error greater than 0.003 were discarded. Finally, a regional test range was applied by comparing the obtained concentrations to a minimal and a maximal acceptable value (*RangeMin and RangeMax*, respectively). At each depth, and over a 1° grid encompassing the whole Med, the *RangeMin and RangeMax* values were obtained from annual climatologies by applying (equations (3) and (4)).

$$RangeMax = Clim \ . \ (1+0.3) \tag{3}$$

$$RangeMin = \min\left(Clim \ .(1-0.3), \max\left(-2, \frac{Clim.(1-0.3) \ + \ 2)}{1000-250} . \ (P+250)-2\right)\right) \tag{4}$$

where *Clim* is the climatological value calculated as the mean in a 1° latitude longitude grid in the depth range 900–1100 m and *P* is the pressure (see supporting information S3 for graphical representation). From the above, more or less 30% variability is accepted around the deep value. The quality control removed 2.5% of the total data set.

### 3.3. Detection Limit

The limit of detection given by the manufacturer is $\sim$2 $\mu M$ (http://satlantic.com/node/355), and it is determined as 3 times the standard deviation of the blank $[NO_3]$. A precise quantification of the measurement accuracy, after the procedure presented above, is difficult because reference measurements from bottle samples are too scarce. However, consistently to the manufacturer procedure, we calculated 3 times the standard deviation of a subset of data containing only surface measurements (0–30 m) from May to October, when $[NO_3]$ values are theoretically 0 $\mu M$ in surface [*Lavigne et al.*, 2013]. Using an important number of data points (1153), we obtained a detection limit of $\sim$1 $\mu M$. Thus, it can be argued that the calibration procedures improved the accuracy given by the manufacturer by a factor of 2.

## 4. Results

### 4.1. Climatological Nitrate Concentrations at Basin Scale

The spatial distribution of $[NO_3]$ at 1000 m depth ($[NO_3]_{deep}$) obtained from the historical database confirms most of the previous findings on the Med $[NO_3]$ field. The more relevant feature is the well-known west-east gradient of decreasing concentrations [*Manca et al.*, 2004; *Moutin and Prieur*, 2012; *Pujo-Pay et al.*, 2011]. Mean concentration at 1000 m depth is 8.1 $\pm$ 0.7 $\mu M$ in the western basin and 5.0 $\pm$ 0.7 $\mu M$ in the eastern basin. $[NO_3]_{deep}$ values are particularly low in the Aegean Sea (north of the Cretan island) with concentrations under 4 $\mu M$. The seasonal variability was studied in the four selected areas (NW Med, TYR, ION, and LEV Figure 2), by calculating monthly climatological values of $[NO_3]$ (averaging values regardless of the year) at both surface (in the 0–30 m layer, $[NO_3]_{surf}$, Figure 3a) and depth (900–1100 m layer,

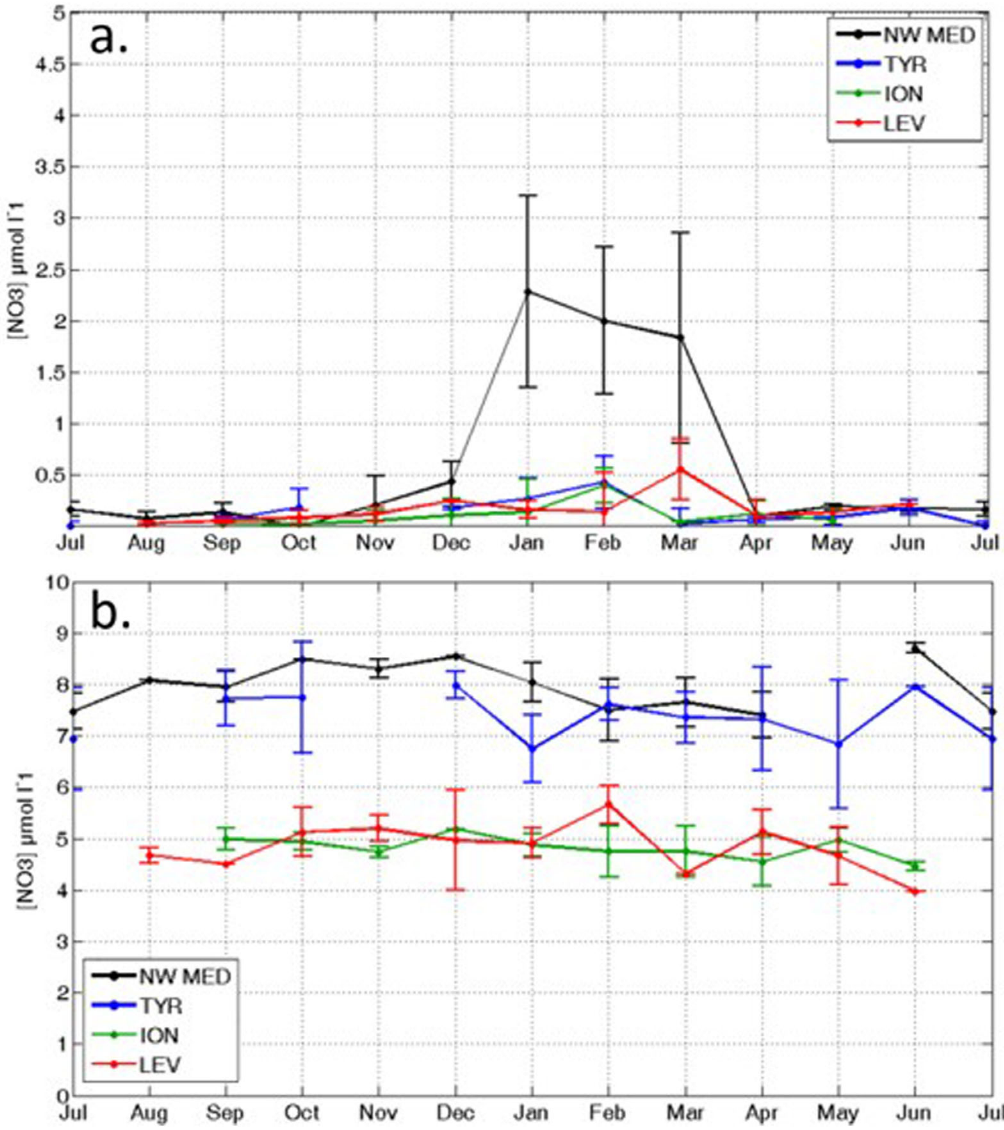


**Figure 3.** Composite times series of [$NO_3$] calculated from the historical database (a) in surface and (b) at depth. The error bar is computed as 2 times the standard deviation.

[$NO_3$]$_{deep}$, Figure 3b). Data from the Aegean Sea were discarded to prevent any artifactual bias related to this area.

In the NW Med, [$NO_3$]$_{deep}$ are almost constant over time even if summer/fall concentrations are slightly higher than during winter/spring. On the other hand, seasonality is observed in surface. [$NO_3$]$_{surf}$ increase is observed in November/December (Figure 3a), with 18 and 29% of the available profiles exceeding 0.5 $\mu M$, respectively, Table 3). At the surface, maximum values are retrieved in January, and concentrations remain high in February and March (2 $\mu M$ on average, and 15% of the profiles exceeding 4 $\mu M$ in surface), to fall down in April and for the rest of the year ([$NO_3$]$_{surf}$ always under 0.5 $\mu M$). The variability (i.e., error bars around mean values) is generally low, except from November to March, indicating an important variability in the measured [$NO_3$]$_{surf}$ during this period. A similar pattern (i.e., [$NO_3$]$_{surf}$ increase in winter-early spring and [$NO_3$]$_{surf}$ $\sim$0 $\mu M$ otherwise) is also observed in the other regions, although with slight differences in the timing, the duration and even more the intensity of the increase. In the TYR and ION, median values of [$NO_3$] slightly increase at surface during January and February, which suggests that limited inputs can be observed, depending on the year. Indeed, 15% (January) and 33% (February) of the surface data exceed 0.5 $\mu M$ for the TYR, and 30% of the data (both January and February) in the ION (Table 3). In the LEV, the

**Table 3.** Number of Nitrate Concentration Profiles in the Database for Each Zone (NW Med, TYR, ION, and LEV) and Each Month, and Proportion of Profiles With Nonnil Nitrate Concentration in Surface

| | NW Med | | TYR | | ION | | LEV | |
|---|---|---|---|---|---|---|---|---|
| | $[NO_3]_{surf} > 0.5$ $\mu M$ (%) | Available Profiles | $[[NO_3]_{surf} > 0.5$ $\mu M$ (%) | Available Profiles | $[NO_3]_{surf} > 0.5$ $\mu M$ (%) | Available Profiles | $[NO_3]_{surf} > 0.5$ $\mu M$ (%) | Available Profiles |
| JAN | 94 | 18 | 15 | 13 | 26 | 34 | 0 | 3 |
| FEB | 100 | 13 | 33 | 3 | 33 | 3 | 14 | 7 |
| MAR | 97 | 33 | 0 | 4 | 0 | 1 | 66 | 3 |
| APR | 0 | 5 | 0 | 5 | 0 | 24 | 0 | 17 |
| MAY | 0 | 7 | 0 | 19 | 0 | 38 | 0 | 1 |
| JUN | 0 | 3 | 0 | 11 | | 0 | 0 | 1 |
| JUL | 0 | 3 | 0 | 5 | | 0 | | 0 |
| AUG | 0 | 8 | | 0 | | 0 | 0 | 3 |
| SEP | 0 | 36 | 0 | 26 | 0 | 14 | 0 | 2 |
| OCT | 0 | 10 | 5 | 54 | 0 | 9 | 0 | 30 |
| NOV | 18 | 11 | | 0 | 0 | 14 | 0 | 9 |
| DEC | 29 | 7 | 0 | 7 | 0 | 2 | 0 | 1 |

increase in surface is delayed of 1 month: values greater than 0.5 $\mu M$ are observed in February and March (14 and 66%, respectively). With the exception of these periods (January/February for TYR and ION, February/March for the LEV), the percentage of $[NO_3]_{surf}$ values exceeding 0.5 $\mu M$ is 0% during the rest of the year. Again, $[NO_3]_{deep}$ are generally constant over time (even slightly decreasing in winter/spring period in the TYR, as for the NW Med), but the dispersion of data hides any clear seasonal pattern.

The first depth of the isocline 1 $\mu M$ was also calculated and considered as a proxy of the nitracline depth ($Z_{NO3}$) [*Lavigne et al.*, 2013; *Van Wambeke et al.*, 2009]. The choice of the threshold value is rather arbitrary, but in accordance with the detection limit ($\sim$1 $\mu M$). Thus, in the following, $Z_{NO3}$ is assumed to separate upper nitrate-depleted waters from lower nitrate-richer waters. The observed west-to-east gradient in the $[NO_3]_{deep}$ distribution is logically reflected in the summer $Z_{NO3}$ (calculated from May to September, Figure 4a). $Z_{NO3}$ median values are relatively constant around 60–80 m in the western basin (0°E–13°E), to sharply increase (around 150 m) in the eastern basin, with the absolute maximum observed in the easternmost regions of the basin (>25°E). The maximum variability in the nitracline depth is observed in the Ionian Basin (between 15° and 20° latitude), keeping in mind that the number of observations is very low. The shape of the $[NO_3]$ gradient is also pertinent to characterize the nitracline [*Omand and Mahadevan*, 2015]. Thus, the slope of the nitracline (see legend of Figure 4 for definition) was also computed, and, not surprisingly, we observed a weakening of the gradient from west-to-east, by a factor of 10.

### 4.2. The $[NO_3]$ Field at High Temporal Resolution: 2013–2014 Period

#### 4.2.1. The North Western Mediterranean Sea: lovbio017b

From June to August 2013, the MLD (calculated using a 0.03 kg m$^{-3}$ density criterion) [*D'Ortenzio et al.*, 2005; *de Boyer Montégut et al.*, 2004], observed by the float in the NW Med was permanently shallow (MLD $\sim$19 m, Table 4). Surface water was totally nitrate depleted over about 60 m depth, with a $[NO_3]_{surf}$ under the detection limit (Figures 5a and 6a). Later, from September to November 2013, the mixed layer progressively deepened and the $Z_{NO3}$ decreased concomitantly to be around 40 m in November 2013. During this period, an isopycnal uplift was also observed, and the deep nitrate reservoir was found closer to the surface (although $[NO_3]_{surf}$ are maintained permanently low). Conditions dramatically changed in December, when an intense increase of the $[NO_3]_{surf}$ was observed. Surface concentrations were approximately 5–6 $\mu M$, decreasing only in late February 2013 (Figures 5a and 6a). During the same period (December–February), a succession of mixed layer deepening events was also observed, at a time scale shorter than a month. The mixed layer extended constantly deeper than the $Z_{NO3}$, as the latter was permanently observed at surface. The MLD reached an annual maximum value of 242 m on 4 February 2014. In March–April, the mixed layer progressively shallows, although deepening events still occurred. $[NO3]_{surf}$ was concomitantly decreasing, and a sharp deepening of the $Z_{NO3}$ was observed, punctuated, however, by events of MLD deepening that, again, reached the $Z_{NO3}$. If seasonal and short time scale $[NO_3]$ values were highly variable at surface, $[NO_3]$ at depth was stable all along the time series. Below 500 m depth (Figures 5a and 6b), $[NO_3]$ was permanently stable around ($\sim$8.6 $\mu M$) for most of the time series. At subsurface layers (150–500 m), and despite

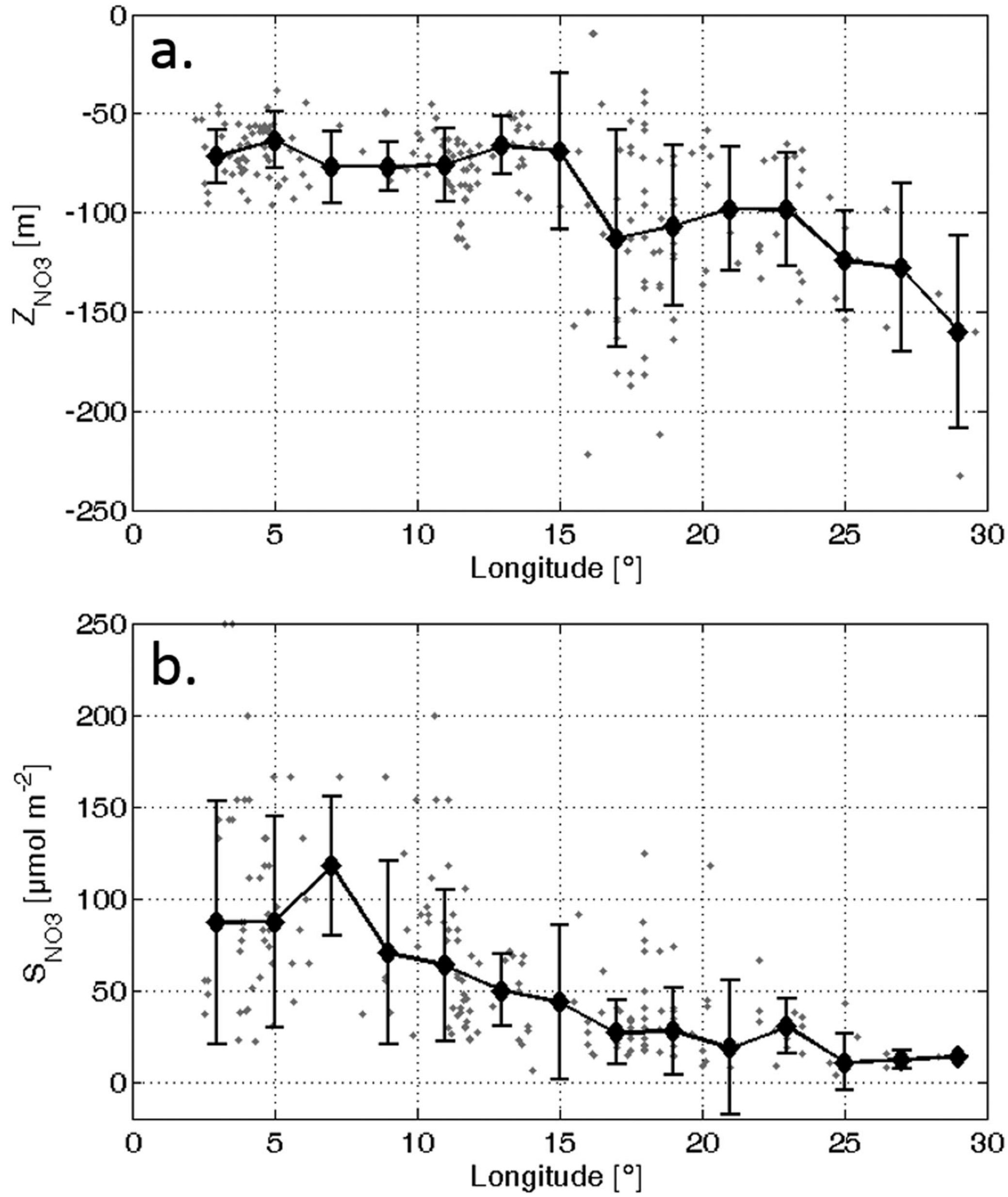


**Figure 4.** Climatological summer (a) nitracline depth ($Z_{NO3}$) and (b) nitracline slope, plotted as a function of the longitude. Grey points figure all the available observations, black circles the median values in 2° longitude boxes, and error bars are determined from the standard deviation (2 standard deviation length). The nitracline slope was evaluated as the vertical [$NO_3$] gradient between the isocline 1 μ*M* and the isocline 3 μ*M*.

mixing events that modified episodically the concentrations, [$NO_3$] field was also constant and with values practically equal to those measured at depth (~8.2 μ*M*).

#### 4.2.2. The Tyrrhenian Sea: lovbio039b and lovbio042c

Covering only the summer-to-winter transition in 2013–2014, the time series acquired in the TYR is the shortest among these of the Mediterranean Bio-Argo floats. From June to August, a thin and stable MLD was observed (Figure 5b and Table 4), and $Z_{NO3}$ was shallow, around 80 m depth. From September to November, MLD progressively extended, from 10 to 55 m, and the vertical distance between $Z_{NO3}$ and MLD decreased (as $Z_{NO3}$ was constant). Later, from December to February, the mixed layer was still deepening, although episodic events of stratification occurred, as shown by the shallow MLD mean value (38 m). During this period, the maximum observed MLD (75 m) was close to the depth of $Z_{NO3}$. The two interfaces (MLD and $Z_{NO3}$) were then very close, though never crossing, during the whole period November–February. As a

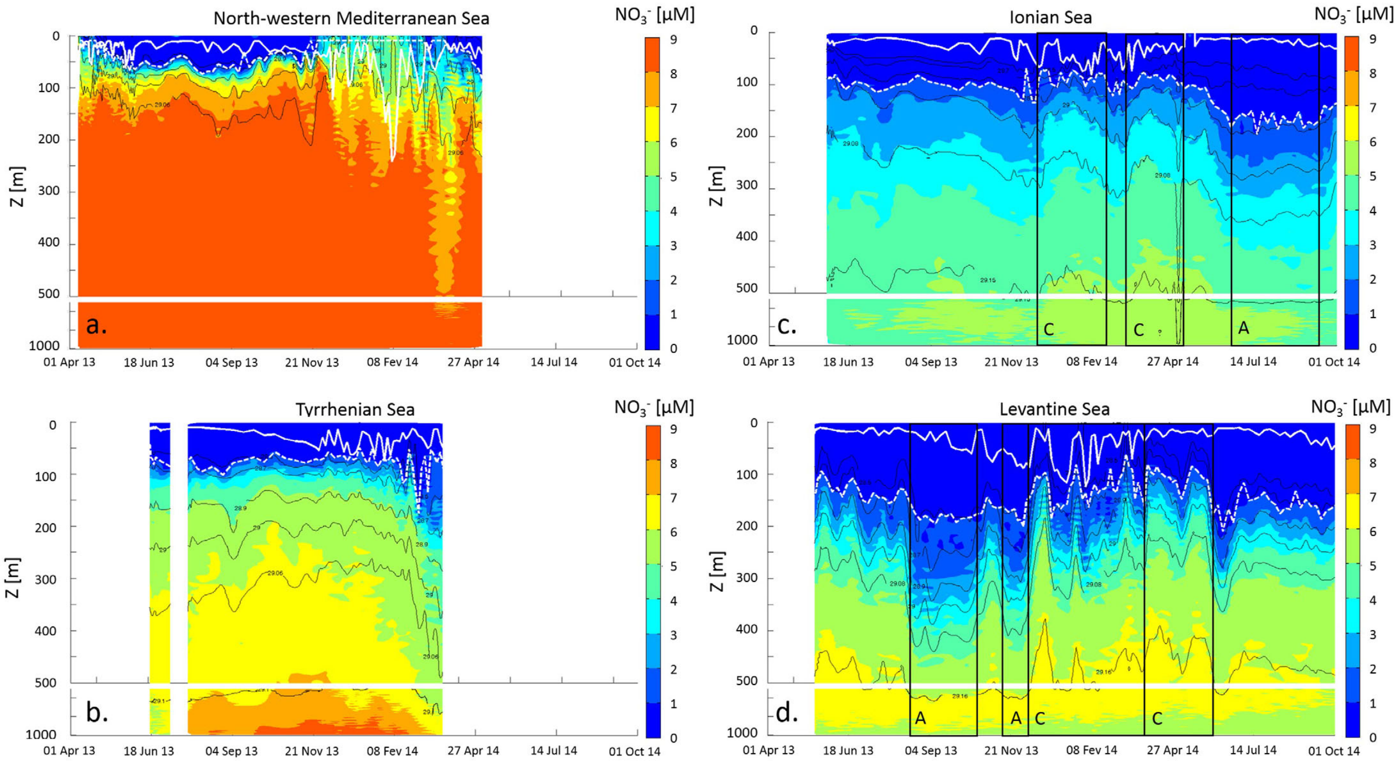


**Figure 5.** [$NO_3$] float transects in (a) the NW Med, (b) TYR, (c) ION, and (d) LEV. Data are interpolated onto a regular grid (1 day × 1 m) with a triangle-based cubic interpolation. Contour plots of density anomalies (28.5, 28.7, 28.9, 29.0, 29.06, 29.12, 29.16, black line), mixed layer depth (solid white line), and nitracline depth (dashed white line) are superimposed. Anticyclonic and cyclonic structures that are discussed in the text are indicated by letters A and C, respectively.

consequence, the deep $NO_3$ stock was never reached by mixing processes, neither occasionally, and surface waters exhibit very low and constant $[NO_3]_{surf}$ values ($[NO_3]_{surf}$ < detection limit). At subsurface layers (100–300 m) and, more generally, below the $Z_{NO3}$, [$NO_3$] is temporally constant, until early March. Then, the float approached coasts, which generated a general isopycnal deepening, and [$NO_3$] at depth shifted from 8 to less than 7 $\mu M$.

#### 4.2.3. The Ionian Sea: lovbio016c

The lovbio016c float deployed in the ION basin observed a shallow MLD all along the considered year (Figure 5c). From June to November 2013, the very low MLD was paralleled by a deep $Z_{NO3}$, located around 130–140 m-depth (Table 4). $[NO_3]_{surf}$ was also very low (under the estimated detection limit, Figure 6a). From late November 2013, the MLD evolution became more chaotic: it extended regularly (with a maximum value, of 82 m, Table 4), although events of shallow MLD were observed. During this period, $Z_{NO3}$ was relatively stable ($Z_{NO3}$ mean value around 100 m over the November–February period, Table 4) and close to MLD, although the two interfaces remained separated. No increase in $[NO_3]_{surf}$ was observed ($[NO_3]_{surf}$ still under detection limit). Two episodes were detected: the first one occurring in late November, and the second in late January. In both cases, subsurface [$NO_3$] increased, to be higher than 4 $\mu M$ at 300 m depth. In April, the MLD progressively decreased, to stabilize during the rest of the time series (summer 2014). In May 2014, however, another change in the characteristics of the water columns was observed, clearly identified by the deepening of the isopycnals and of the $Z_{NO3}$ depth. Stable values were again observed in October (and in November/December, not shown), when the float escaped from this third structure.

All along the time series, $[NO_3]_{surf}$ were low, and their distribution over the 50 first meters was relatively unaffected by the seasonal (atmospherically driven) forcing. On the other hand, the main variations were all observed in the subsurface layers.

#### 4.2.4. The Levantine Sea: lovbio018c

During summer 2013 (June–August), the lovbio018c float, deployed in the LEV basin, observed a shallow and constant MLD, with an average value of about 18 m. In September–December, the mixed layer progressively deepened, though during several consecutive events, shallow MLDs were recorded. In January, the MLD

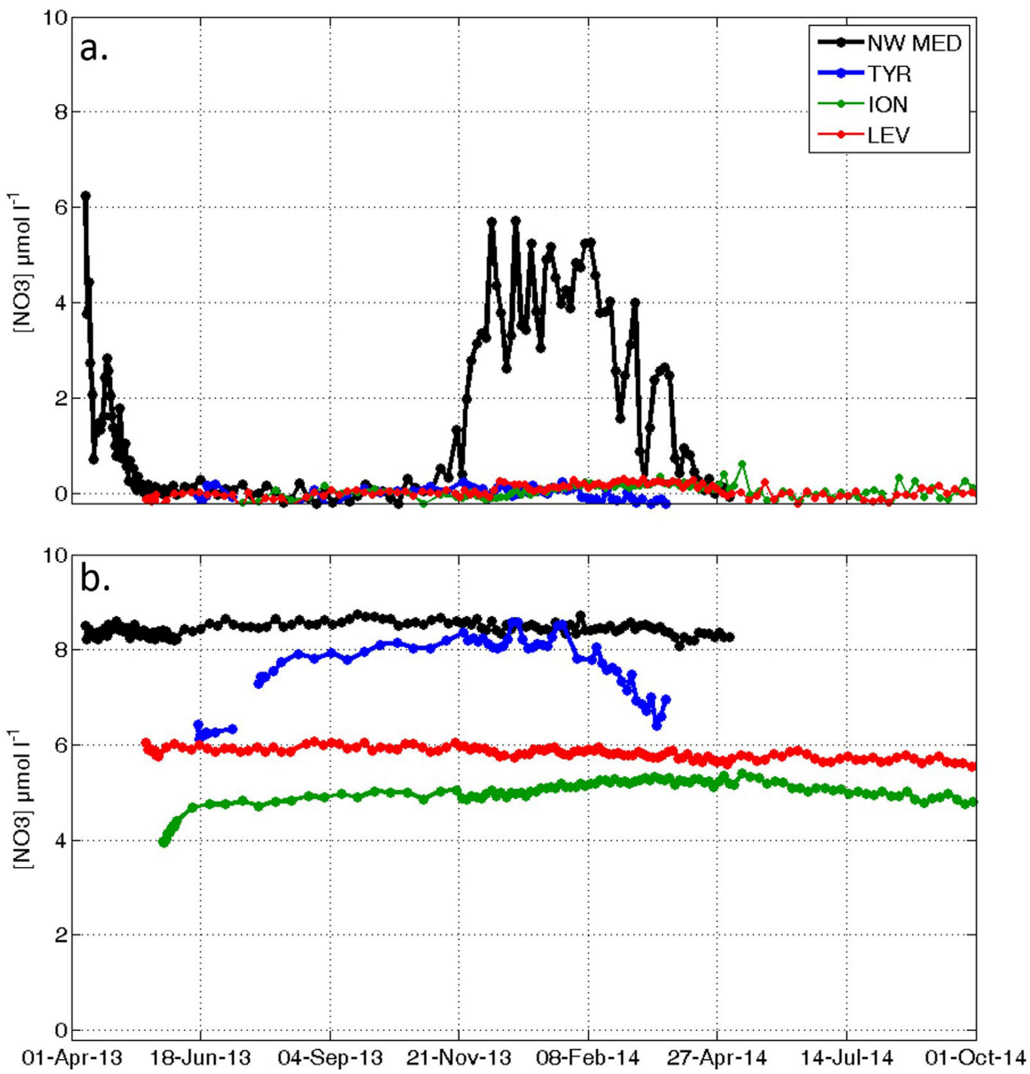


**Figure 6.** [$NO_3$] float times-series (a) in surface layer (0–30 m) and (b) at depth (900–1100 m).

reached its annual maximum (124 m), with also a high mean value (65 m, Table 4). During the winter period, the mean temporal trend of $Z_{NO3}$ was decreasing, resulting in a reduced distance between the two interfaces (i.e., MLD and $Z_{NO3}$). However, they never crossed, and, consequently, [$NO_3$]$_{surf}$ was durably under the detection limit. After its annual maximum in February, the MLD decreased, to be permanently shallow from March and for the rest of the time series (Figure 5d). $Z_{NO3}$ was more variable, though, it was observed between 100 m (winter) and 150 m (spring and summer), on average. Overall, [$NO_3$]$_{deep}$ was very stable and around 5 µ*M* (Figure 6b), whereas [$NO_3$]$_{surf}$ was permanently lower than the estimated detection limit (Figure 6a). However, important fluctuations around the mean values were observed for MLD and $Z_{NO3}$. They were generally associated with a succession of uplift and downlift of the isopycnals and they coincide to important modifications of [$NO_3$] of the water column, particularly in the subsurface layers (i.e., 100–400 m). From late August to early December, an isopycnal downlift of about 150 m was observed and the [$NO_3$] distribution of the water column was strongly modified. During this period, and apart from 3 weeks in November, [$NO_3$] in subsurface dramatically decreased, to be around 2 µ*M*. From the end of December to the end of April, [$NO_3$] in subsurface increased overall, and pulses of high [$NO_3$] were regularly observed. Note, however, that [$NO_3$]$_{surf}$ was permanently under the detection limit during these events. For the rest of the considered time series, the float followed the bathymetric isoline of 1500 m, flowing all along the Egyptian coasts (Figure 2). [$NO_3$] values came back to the level observed at the beginning of the time series (i.e., June 2013), and also their vertical distributions were similar, with a stable $Z_{NO3}$ at about 150 m.

**Table 4.** Seasonal Characteristics of Float Transects[a]

| | | $MLD_{mean}$ (m) | $MLD_{max}$ (m) | $Z_{NO3mean}$ (m) |
|---|---|---|---|---|
| NW Med | Jun–Aug | 19 ± 10 | 47 | 57 ± 10 |
| | Sep–Nov | 29 ± 12 | 64 | 40 ± 18 |
| | Dec–Feb | 70 ± 60 | 242 | 0 ± 0 |
| | Mar–May | 29 ± 22 | 124 | 30± 19 |
| TYR | Jun–Aug | 12 ± 1 | 16 | 84 ± 10 |
| | Sep–Nov | 32 ± 13 | 55 | 73 ± 6 |
| | Dec–Feb | 38 ± 17 | 75 | 74 ± 18 |
| | Mar–May | 34 ± 14 | 51 | 90± 40 |
| ION | Jun–Aug | 16 ± 4 | 26 | 138 ± 35 |
| | Sep–Nov | 31 ± 10 | 54 | 131 ± 25 |
| | Dec–Feb | 45 ± 18 | 82 | 100 ± 23 |
| | Mar–May | 31 ± 16 | 74 | 93 ± 10 |
| LEV | Jun–Aug | 19 ± 6 | 35 | 151 ± 23 |
| | Sep–Nov | 49 ± 18 | 85 | 171 ± 13 |
| | Dec–Feb | 65± 35 | 124 | 145 ± 32 |
| | Mar–May | 22 ± 12 | 72 | 110 ±22 |

[a]Column 1: mean value of the MLD, column 2: maximum value of the MLD, and column 3: mean value of $Z_{NO3}$.

## 5. Discussion

### 5.1. Seasonal Patterns

The sequence of events characteristic of a temperate sea regime (i.e., fall-winter mixing, spring primary production, and no mixing in summer) [*Sverdrup et al.*, 1942] is observed in the NW Med. In the analysis of the historical data set, it appears particularly persistent, too (Figure 3a and Table 3), at least at the temporal resolution of the used data. Indeed, the percentage of profiles with nonzero values at surface during the period of January–March is close to 100% (94% in the January, 100% in February, 97% in March, Table 3), and from April to November, the percentage is constantly 0%. The data of the float lovbio017b confirm this general pattern, during the 2013–2014 period, although limited to a more restricted area. To assess the spatial representativeness of these data, the float trajectory was compared to the bioregions obtained by clustering satellite surface chlorophyll time series [*D'Ortenzio and Ribera d'Alcalà*, 2009]. We verified that all the profiles of the lovbio017b float were unambiguously obtained in a unique area (i.e., the "Bloom" bioregion in the *D'Ortenzio and Ribera d'Alcalà* [2009] classification), suggesting that profiles could be reasonably considered representative of the whole bioregion.

On the basis of these data, the role of the winter deep MLD in the whole NW Med, which is generally evoked to explain the high $[NO_3]_{surf}$ values in winter [*Gačić et al.*, 2002; *Lavigne et al.*, 2013; *Marty et al.*, 2002], should be reexamined. Increase of the $[NO_3]_{surf}$ was, in fact, observed, despite a shallow MLD and without deep convection (during which a complete homogenization of the water column can be observed, e.g., in winter 2012) [*D'Ortenzio et al.*, 2014; *Durrieu de Madron et al.*, 2013]. In addition, the depth reached by the mixed layer seemed to poorly determine the resulting mean quantity of available $NO_3$ in surface (Figures 5a and 6a). Indeed, relatively shallow MLD (i.e., greater than 80 m) should be able to trigger high $[NO_3]_{surf}$ and 50% of the $NO_3$ supply potentially occurs in the first 200 m. A possible explanation has been recently proposed [*D'Ortenzio et al.*, 2014], and it is related to the permanent cyclonic circulation of the NW Med that maintains high $[NO_3]$ in subsurface layers in early winter [*Robinson et al.*, 2001]. Shallow summer $Z_{NO3}$ (~60–80 m on average, Figures 4a and 5a) and strong $[NO_3]$ vertical gradient observed in the NW Med (~100 $\mu$mol $m^{-4}$, Figure 4b) seems then to play a role at least as important as the winter MLD in controlling the $NO_3$ supply to the surface layer in winter. There is a point, however, that demands a deeper analysis. If the temporal evolution is similar between the historical database and float observations, the absolute values of $[NO_3]_{surf}$ in winter are different (the historical database showing systematically lower values than those from float). The monthly resolution of the database, as well as the averaging procedures, might explain the difference: if only values of $[NO_3]_{surf} > 4$ $\mu M$ are accounted during the December–March period, 15% and 35% profiles are observed, respectively in the historical database and in the float data. The historical database is probably biased by undersampling in situations of high $[NO_3]_{surf}$, which are directly generated by severe weather conditions.

In the TYR region, the climatological winter MLD [*D'Ortenzio et al.*, 2005; *Houpert et al.*, 2015] may potentially reach the climatological summer $Z_{NO3}$ (around 60 m, Figure 4a). However, $[NO_3]_{surf}$ are fairly constant and around 0 $\mu M$ in the historical data set (Figure 6a), indicating that the increase of $[NO_3]$ in surface layers, even episodic, is not relevant. During the limited period of float observations, no increase in $[NO_3]_{surf}$ was observed, indeed (Figures 5b and 6a), and summer $Z_{NO3}$ was found deeper than the annual maximum MLD value (Table 4). The interplay between MLD and $Z_{NO3}$ interfaces in the TYR appears then unable to provide an efficient nutrient supply at surface, but it cannot be excluded that, some years, seasonal processes could be determinant, thanks to a shallow and steep nitracline. Historical and float data seemingly confirm the classification of the TYR as a subtropical regime proposed by *D'Ortenzio and Ribera d'Alcalà* [2009], even if the float was episodically located in an "Intermittently" bioregion (bioregion #4 in *D'Ortenzio and Ribera d'Alcalà* [2009]). The limits of our data (low temporal resolution for the climatology and very short time series for the float) leave the question still open.

In the eastern basin (i.e., ION and LEV areas), the analysis of the historical data set evidences $[NO_3]_{surf}$ around 0 $\mu M$ all along the year (Figure 3a), which is typical of subtropical-like regimes, where the seasonality of surface $[NO_3]$ is less marked [*Henson et al*., 2009; *Mann and Lazier*, 2009; *Menzel and Ryther*, 1960; *Steinberg et al*., 2001], and, for the most, related to internal waves [*Cullen et al*., 2002] or by episodic events (as mesoscale oceanic structures [*Johnson et al*., 2010; *McGillicuddy et al*., 1998; *McGillicuddy et al*., 2007] or atmospheric perturbations, i.e., cyclones or storms [*Bates et al*., 1998; *Nelson*, 1998]). At climatological scale, winter MLD is around 100 m in the ION and 125 m in the LEV [*D'Ortenzio et al*., 2005; *Houpert et al*., 2015], and $Z_{NO3}$ lies generally too deep to be reached by the seasonal MLD overturning (Figure 4a). Thus, in the eastern basin, the probability that MLD is deeper than $Z_{NO3}$ is low [*Lavigne et al*., 2013], limiting the possibility of an efficient $NO_3$ supply to the surface, all the more so as the $[NO_3]$ increase below $Z_{NO3}$ is weak ($\sim$10 $\mu$mol m$^{-4}$, Figure 4b). Float data, introduced here, all located in "No Bloom" bioregions (bioregions #1, #2, and #3 in *D'Ortenzio and Ribera d'Alcalà* [2009]), corroborate most of these findings. In general, float observations confirmed that winter MLD deepening events in the eastern basin were not intense enough to supply large amounts of $NO_3$ close to surface (at least during the 2013/2014 period). Moreover, the mean $Z_{NO3}$ was always found deeper than the maximum winter MLD (Table 4), and even when the mean winter MLD (65 m) was comparable to the one observed in the NW Med (70 m), as in the LEV, the $Z_{NO3}$ was never reached. However, the threshold values selected to estimate the depth of the interfaces (i.e., MLD and $Z_{NO3}$) may bias these results. The sensitivity of the nitracline to the 1 $\mu M$ criterion was therefore assessed by considering a change by 50% on the selected threshold value (i.e., by considering a criterion varying from 0.5 to 1.5 $\mu M$). For the float data set, it results in a mean depth change of 8, 26, 39, and 71 m for the NW Med, TYR, ION, and LEV, respectively. The sensitivity of $Z_{NO3}$ to the selected threshold value is then increasing eastward, as a consequence of a sharper gradient in the western basin than in the eastern one. However, it concerns less than 1.5% of the $NO_3$ stock from 0 to 1000 m depth, in both eastern and western basins. Thus, since increases in $[NO_3]_{surf}$ were never observed in the ION and LEV time series, the MLD was truly never crossing the $Z_{NO3}$, or, at least, only episodically, and, in any case, not enough to bring large amounts of nutrients to the surface layers. In others words, the deep $NO_3$ stock in the eastern Med regions is permanently out of reach of the seasonal MLD overturning.

### 5.2. Role of High-Frequency Processes in Shaping the $[NO_3]$ Seasonal Cycle

#### 5.2.1 MLD Deepening Events in the NW Med

The comparative analysis between historical data set and float data demonstrated that the seasonal pattern of $[NO_3]$ in the NW Med is strongly affected by high-frequency (i.e., between days and months) processes. In particular, float data showed (Figure 6a, black line), that mechanisms controlling $[NO_3]_{surf}$ are not continuous and constant processes. Conversely, they are driven by episodic and intense mixing processes, characterized by a succession of events lasting several days. Highly frequency events are not detected in the climatological analysis (i.e., Figure 3a) as they are, by their very nature, difficult to sample by ship. Most of them were associated with an increase in $[NO_3]_{surf}$, and $[NO_3]_{surf}$ is maintained high, supported by regular MLD deepening events. Entrainment pulses of $NO_3$ into the euphotic layer by MLD deepening events were estimated (equation (5)).

$$Nsup(t)=\left[\int_0^{MLD(t+\Delta t)} NO_3(z,t)\ dz\ .\ \frac{Zeu\ (t+\Delta t)}{MLD(t+\Delta t)}\right]-\left[\int_0^{Zeu(t)} NO_3(z,t)\ dz\right] \quad (5)$$

In equation (5), $NO_3(t,z)$ is the $[NO_3]$ at a given depth, and for the profile acquired at time $t$. $Nsup(t)$ corresponds to the quantity of $NO_3$ (expressed in $\mu$mol m$^{-2}$) brought to the photic layer, $Z_{eu}$, which was calculated from PAR profiles and estimated as the 1% light level depth, during the interval time, $\Delta t$ (i.e., between two profiles). The first right-hand term of equation (5) estimates the quantity of $NO_3$ that will be theoretically found in the photic layer at time $t+\Delta t$, assuming homogeneous $[NO_3]$ in the MLD. $Nsup(t)$ is then obtained by subtracting from this value the initial quantity of $[NO_3]$ measured in $Zeu\ (t)$. Note that equation (5) does not take directly into account the $[NO_3]$ profile at time $t+\Delta t$, i.e., there is no assumption on $NO_3$ consumption between two consecutive profiles.

Inputs of [$NO_3$] depend to a large extent on the accuracy of the MLD estimate. Time series of the daily MLD modeled at the DYFAMED site [*Heimbürger et al.*, 2013], by the Symphonie model [*Herrmann and Somot*, 2008; *Marsaleix et al.*, 2008] over the 1995–2008 period, shows that a 3 day sampling may underestimate the MLD value by around 10%. The possible bias introduced by a MLD underestimation on $NO_3$ inputs was taken into account, given that during the well-mixed period the float performs measurements on a 3 day basis.

$NO_3$ inputs are maxima from December to February (4.1–4.9 $10^5$ $\mu$mol m$^{-2}$) and represent about 60 to 70% of the total input by MLD deepening events. March–May period is also marked by the presence of some mixing events that are potentially able to bring nutrients to the surface and maintain high [$NO_3$]$_{surf}$ for several days (e.g., on 20 April 2013, 4 March 2014, and 21 March 2014). However, since the frequency of these events is low and the $Z_{NO3}$ is found deeper, inputs are limited (1.6–2.9 $\times$ $10^5$ $\mu$mol m$^{-2}$ over the period). MLD deepening events of same magnitude can also have different consequences depending on the depth of the nitracline. For example, the MLD deepening event on 20 April 2013 (MLD = 56 m) brought $NO_3$ up to the surface layer owing to a shallow nitracline, whereas the event occurring on 25 May (MLD $\sim$ 58 m) was not associated with an increase in [$NO_3$], due to a deeper nitracline. Overall, the total input of $NO_3$ to the photic layer estimated from the float time series during 2013–2014 period (1 year) ranges from 0.6 to 0.8 mol m$^{-2}$.

The new production triggered by new nitrogen provided to the surface layer by MLD deepening events may be estimated in the range of 49–67 g C m$^{-2}$ (using the standard C:N ratio) [*Redfield*, 1934], which is a typical value for the area [*Severin et al.*, 2014; *Tusseau Vuillemin et al.*, 1998]. When comparing with other physical processes, MLD deepening events appear as the main source of new N to the photic layer (about 100 times higher than the estimated diffusive flux in the area [*Copin-Montégut*, 2000; *Moutin and Raimbault*, 2002], and more than 10 times higher than the atmospheric deposition [*Migon et al.*, 1989; *Pasqueron de Fommervault et al.*, 2015b]. These inputs are strongly determined by the "intermittency behavior" of the MLD that could not be properly resolved with standard measurements. This is a key point because the temporal variability of the nutrient flux is believed to drive the ecosystem response [*Pasquero et al.*, 2005].

#### 5.2.2. Role of Mesoscale in Subsurface Layer

The use of floats represents a step forward with respect to climatological studies. They provide an interpretation of the mean seasonal time series, considered as representative of a bioregion, although they could also identify the impact of small spatiotemporal scale perturbations over this seasonal cycle. The difference in environmental conditions between the Mediterranean regions (temperate sea and subtropical regimes in the NW Med and the eastern basin, respectively) determines, however, the way in which these processes may alter the seasonal dynamics of [$NO_3$]. In the NW Med, we demonstrated in the previous paragraph that the surface variability of [$NO_3$] is great, and, for the most, induced by the seasonal deepening of the MLD related to the atmospheric forcing. The small-scale perturbations are for the most induced by the high-frequency variability of the MLD. In the TYR, the influence of the small-scale perturbations is difficult to identify, as the duration of the time series is relatively too short. It may be stated, however, that the TYR insures exchanges between western and eastern basins [*Krivosheia and Ovchinnikov*, 1973; *Hopkins*, 1988], and that the area is thus characterized by complex circulation. One can mention the presence of different water masses [*Astraldi et al.*, 2002], an intense mesoscale activity [*Astraldi et al.*, 1999, 2002; *Fernández et al.*, 2005; *Rinaldi et al.*, 2010], and the coexistence of three bioregions [*D'Ortenzio and Ribera d'Alcalà*, 2009]. This peculiar situation may result in complex [$NO_3$] vertical distribution [*Ribera d'Alcala et al.*, 2009], likely to modulate the seasonal pattern over short-time scales, but this point cannot be elucidated any further here.

In the eastern basin, most of the variability of [$NO_3$] is observed at depth (below approximately 150 m), indicating an important and permanent decoupling of the surface and subsurface/deep dynamics. The subsurface temporal variability seems closely related to short time scale isopycnal displacement. Indeed, in subsurface ($\sim$300 m) float data for LEV and ION show that the variance on isopycnals is lower than the variance on isobars (Figure 7). In particular, it is up to 32 times smaller in the LEV, where the [$NO_3$] variability is the highest (i.e., [$NO_3$] values at 300 m depth vary from around 2 to 6 $\mu M$, Figure 7a; almost constant around 4 $\mu M$ for [$NO_3$] at a fixed density, Figure 7b). Such a coorientation of [$NO_3$] with density is often observed because dynamical processes that vertically displace water masses with their properties are generally strong, compared to the biological pump [*Ascani et al.*, 2013; *Omand and Mahadevan*, 2013; *While and*

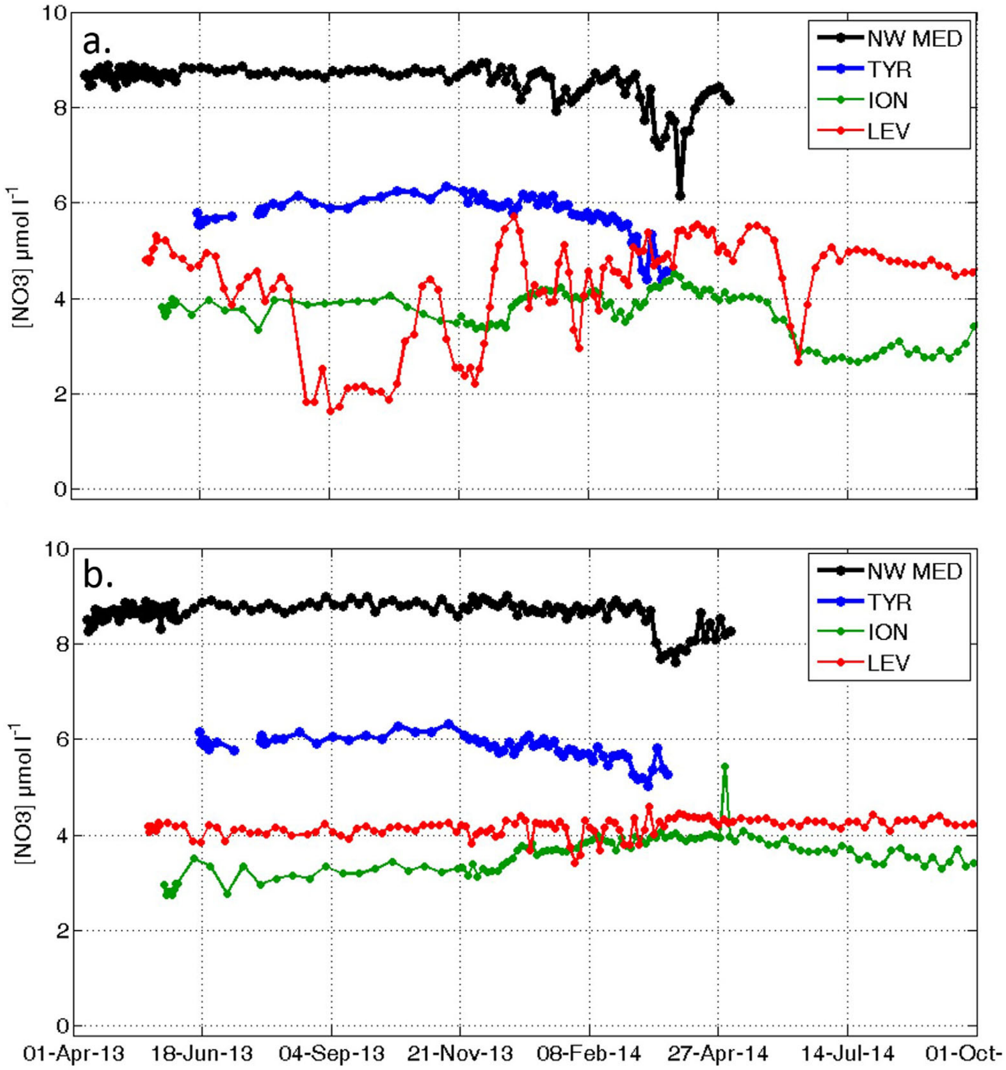


**Figure 7.** [$NO_3$] float times series in the intermediate layer (i.e., 300 m): (a) along isobar 300 m and (b) along isopycnals. Isopycnal values were chosen for each time series in order to correspond to the average density value over the 250–350 m-depth layer (i.e., 1029.10 kg m$^{-3}$ for the NW Med, 1029.05 kg m$^{-3}$ for the TYR, 1029.08 kg m$^{-3}$ for the ION, and 1029.05 kg m$^{-3}$ for the LEV).

*Haines*, 2010]. The variability of [$NO_3$] on isobars (Figure 7a) is, however, intriguing, as it informs on the increase/decrease of the availability of $NO_3$ in the enlightened layer.

In the ION, the analysis of altimetry-derived maps of SLA (Figure 8) suggests the presence, in the region sampled by the floats, of two different cyclonic structures, typically characterized by local minimum SLA [*Isern-Fontanet et al*., 2003; *Morrow et al*., 2004]. After being entrapped at the end of November (Figure 8b), the float escaped from the first structure, approximately 10 February. The float was then entrapped a second time (likely in a different cyclonic structure, following altimetry data and float trajectory, Figure 8c). During these two events, physical and chemical characteristics of the water column were modified, due to uplift/downlift of isopycnals, associated with cyclonic and anticyclonic eddies, respectively. Even if no increase was observed in surface, subsurface [$NO_3$] values raised to be found around 4 $\mu M$ at 300 m depth (Figures 7a and 10a). A correspondent decrease in temperature and salinity was also observed from the surface and up to 400 m (Figures 10b and 10c). The float definitively escaped from the second structure at the end of April and was then located in a positive SLA area (Figure 8d) for the whole summer period (from early May to the end of September). In this case, and conversely to two previous cyclonic structures, temperature and salinity anomalies are positive and [$NO_3$] decreases in subsurface to reach minimum relative

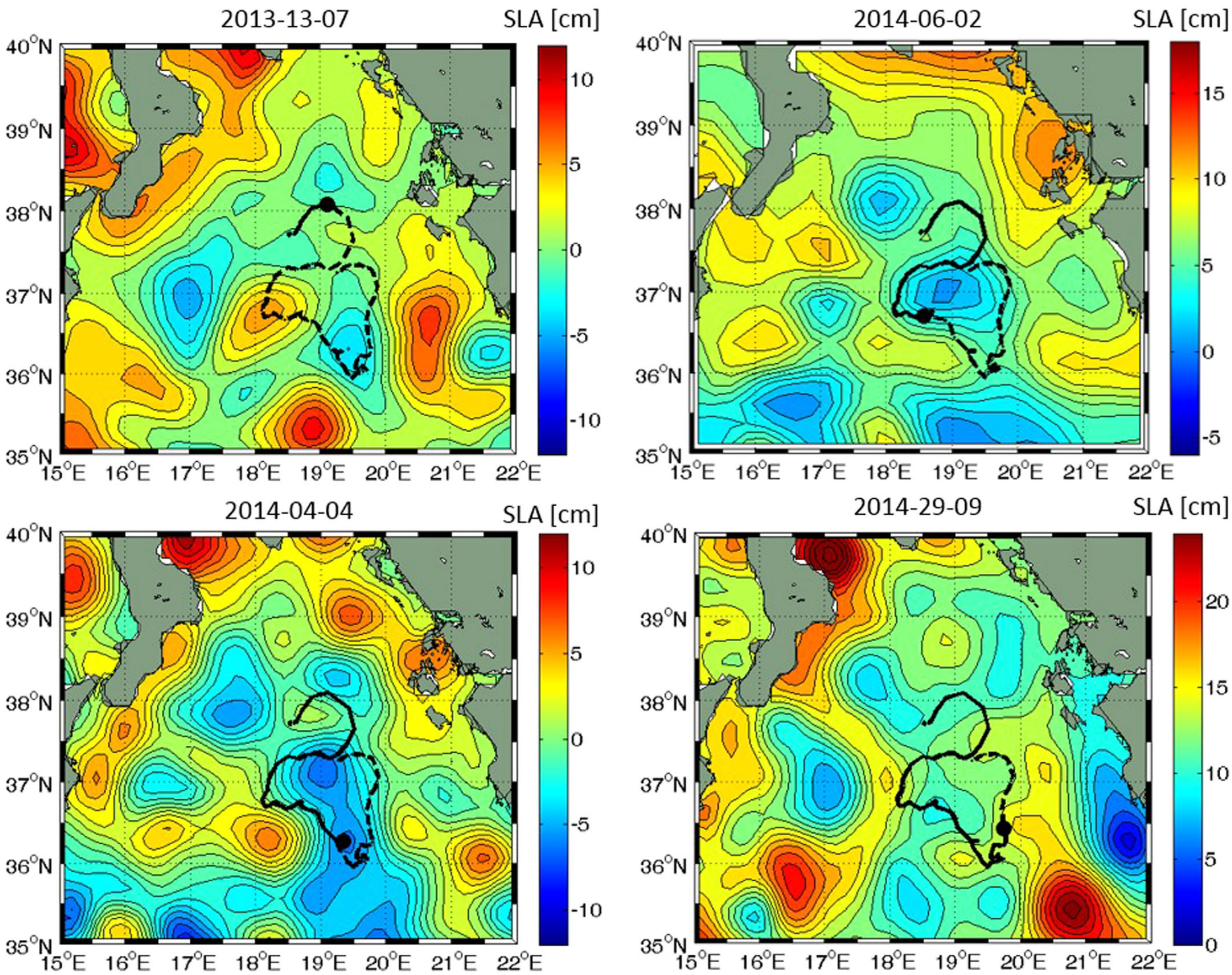


**Figure 8.** Contour plots of sea level anomalies in the Ionian Sea (in red, anticyclonic structures and, in blue, cyclonic structures). The position of the float lovbio016c matching with the altimetric map is represented by a black dot. The solid black line indicates the path before date and the dashed line the path after date.

values (compare blue and red profiles, Figure 10a). Overall, main changes in temperature, salinity, and [$NO_3$] were observed from 100 to 500 m.

The same analysis of altimetry-derived maps conducted in the LEV (Figure 9) confirms the presence of dynamical structures in the vicinity of the float. A first important event was recorded from late August to early December 2013. During this period, the float was entrapped in an anticyclonic structure, as observed by altimetry (Figure 9a), which strongly modified temperature and salinity distributions of the water column. From around 100 to 600 m depth, temperature increased, whereas salinity decreased below 100 m, increasing only from 300 to 600 m (Figures 11b and 11c, red line). Simultaneously, [$NO_3$] significantly decreased in the 100–600 m-depth layer (Figure 11a) as a consequence of an isopycnal downlift. For a limited period (about 3 weeks in November), the float moved to the border of the structure (sampling then slightly higher [$NO_3$] in subsurface, Figure 7a), although it escaped definitively only in December. Successively (from end of December to February), the float moved in a region on the border of a cyclonic structure (Figure 9b). It is striking that when the float approaches the center of the cyclonic structures (i.e., 25 December 2013 and 24 January 2014), peaks are observed in the subsurface [$NO_3$], indicating the general positive feedback of cyclonic structures in nutrient refueling in surface and subsurface (Figure 7a). From March, the float definitely left this cyclonic structure, to be, however, entrapped in a second one, as shown by its trajectory

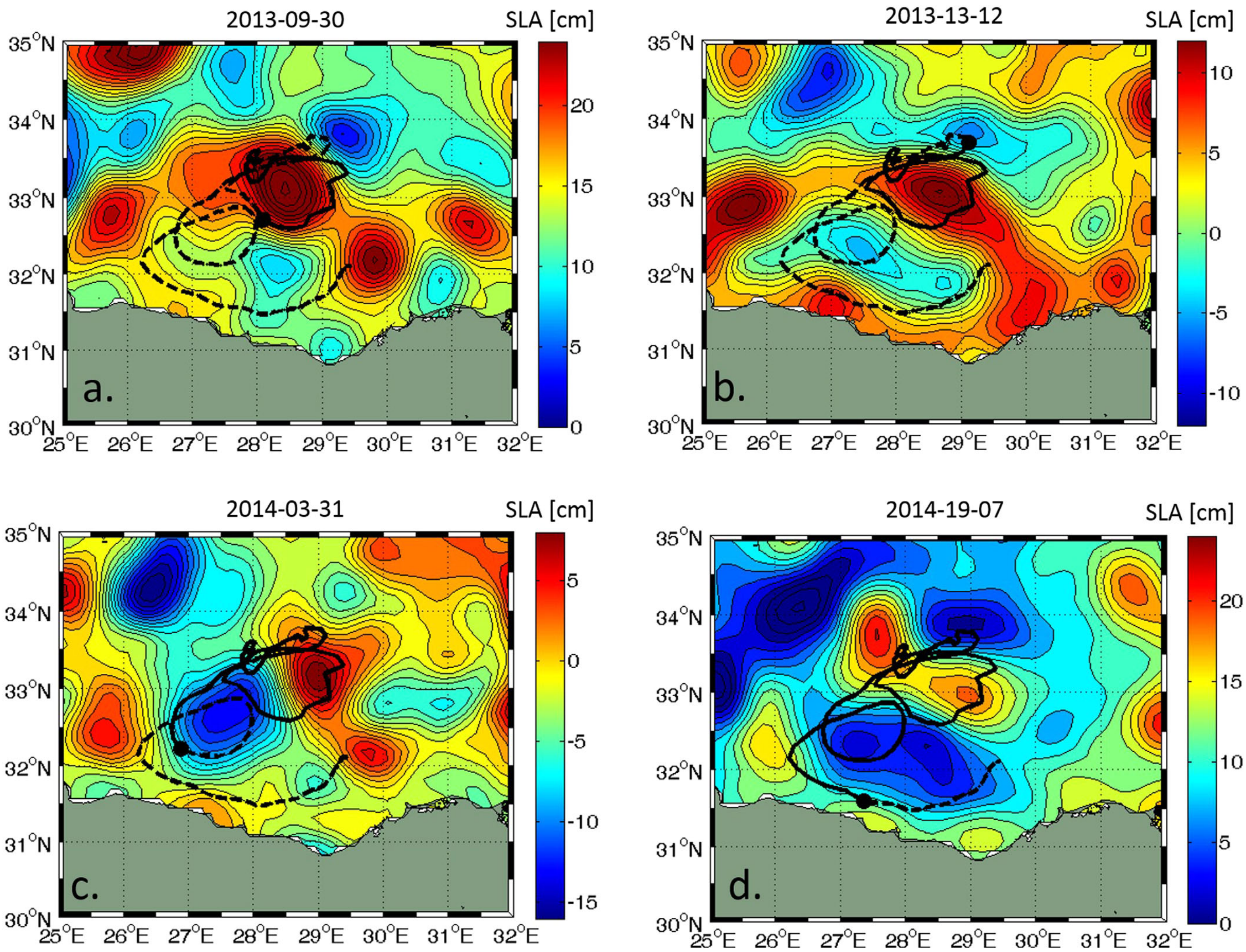


**Figure 9.** Idem as Figure 8, but for the case of float lovbio018c (Levantine Sea).

compared to satellite SLA (Figure 8c). The float finally escaped from the second cyclonic structure at the end of April. These two eddies were typically characterized by low temperature and high salinity in subsurface (Figures 11b and 11c, blue lines).

Overall, in the eastern basin of the Med, the $NO_3$ subsurface variability could be directly explained by the recurrent, though chaotic and episodic, occurrence of mesoscale structures, which are persistently detected in the basin [e.g., *D'Ortenzio et al.*, 2003; *Hamad et al.*, 2006; *Taupier-Letage*, 2008; *Hamad et al.*, 2006; *Millot and Taupier-Letage*, 2005]. Such processes are almost impossible to observe with traditional shipboard hydrographic methods, being too weak and too rapid to be detected, and largely underestimated, on a global scale [*McGillicuddy and Robinson*, 1997; *McGillicuddy et al.*, 1998]. Our data confirm that mesoscale features could be a potential vehicle for nutrient transport in subsurface in oligotrophic environment and then may play an important role in controlling phytoplankton growth in the eastern basin all along the year. This will be further discussed in section 5.3.

### 5.3. Effect of [$NO_3$] Dynamics on [Chl] Distribution

The availability of nutrients is a key point to understand phytoplankton distribution, often estimated from [Chl] measurements [*Cullen*, 1982; *Strickland et al.*, 1969]. In this section, [$NO_3$] and [Chl] float measurements are simultaneously analyzed to assess the impact of [$NO_3$] on the seasonal cycle of [Chl] in the four considered regions.

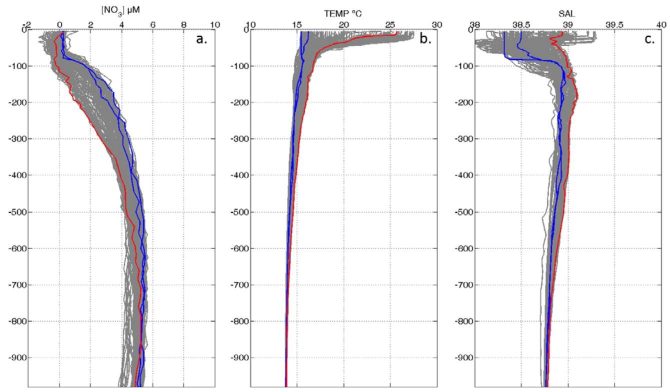


**Figure 10.** Vertical profiles of (a) $[NO_3]$, (b) temperature, (c) salinity, acquired in the ION. Blue and red lines are for cyclonic and anticyclonic structures corresponding to the date of Figure 8, and grey lines represent all the other profiles.

Overall, in all sampled areas, a summer Deep Chlorophyll Maximum (DCM) that deepens eastward is observed and confirms results from previous studies [*Crise et al.*, 1999; *Lavigne et al.*, 2015; *Moutin and Raimbault*, 2002] (Figure 12). In the NW Med, the DCM is observed at depths close to the $Z_{NO3}$ during the summer period (Figure 12a). In autumn, the DCM depth decreases, and the DCM disappears in winter, during MLD deepening events. Phytoplankton cells are likely redistributed over several dozen meters, which leads to an increase in [Chl] surface values. Surface increase occurs together with an increase in total [Chl] that starts when $NO_3$ becomes abundant in surface (i.e., in December). Total [Chl] shifts from 20 to 50–70 mg $m^{-2}$ and remains high throughout the entire winter season, owing to regular $NO_3$ inputs. Rapid decrease in $[NO_3]$ between two successive events confirms that the $NO_3$ stock is consumed in surface during winter and probably sustains phytoplankton production. Note, however, that $[NO_3]$ in surface remains high, suggesting that the $NO_3$ refueling is faster than its uptake by biota. Maximum values are observed in March/April (total Chl $>$ 120 mg $m^{-2}$), concomitantly to a sharp decrease in $[NO_3]_{surf}$. During this period, MLD deepening events occur less frequently, which favors, on the one hand, phytoplankton growth, but limits, on the other hand, $[NO_3]$ inputs. Therefore, in the NW Med, where the MLD reaches $Z_{NO3}$, a spring bloom is observed. Additionally, high-frequency events of MLD deepening during winter also sustain a significant winter production. In the others areas, the winter increase in surface [Chl] is concomitant with the deepening of the MLD. However, no simultaneous increase in total [Chl] was observed, and, therefore, this should not reflect any actual increase in biomass. Indeed, the $Z_{NO3}$ constantly deeper than the MLD confirms that $NO_3$ is not available at surface and that Chl is likely redistributed on the vertical (i.e., it does not result from new production).

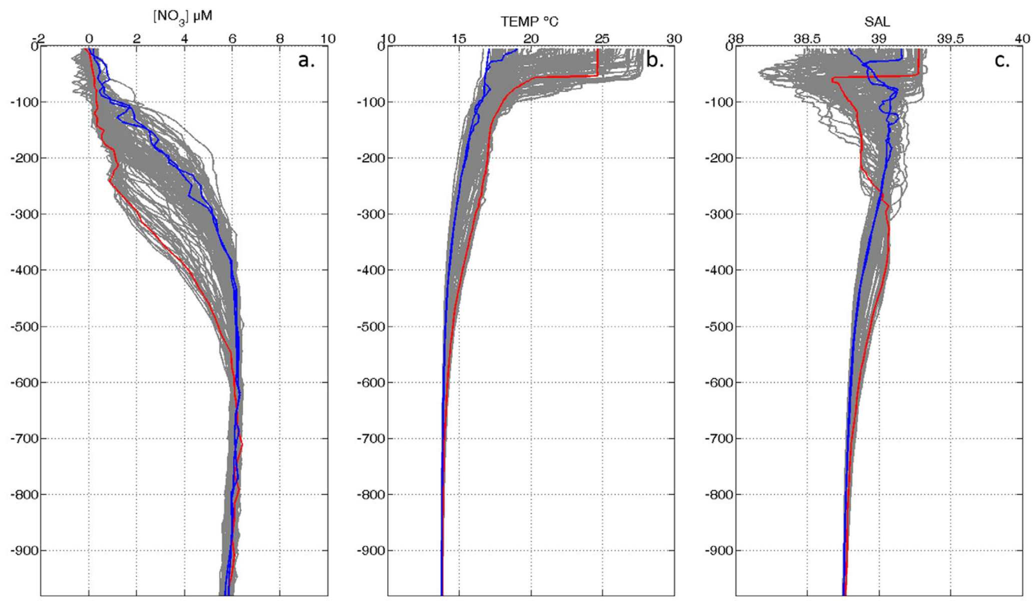


**Figure 11.** Vertical profiles of (a) $[NO_3]$, (b) temperature, (c) salinity, acquired in the LEV. Blue and red lines are for cyclonic and anticyclonic structures corresponding to the date of Figure 9, and grey lines represent all the other profiles.

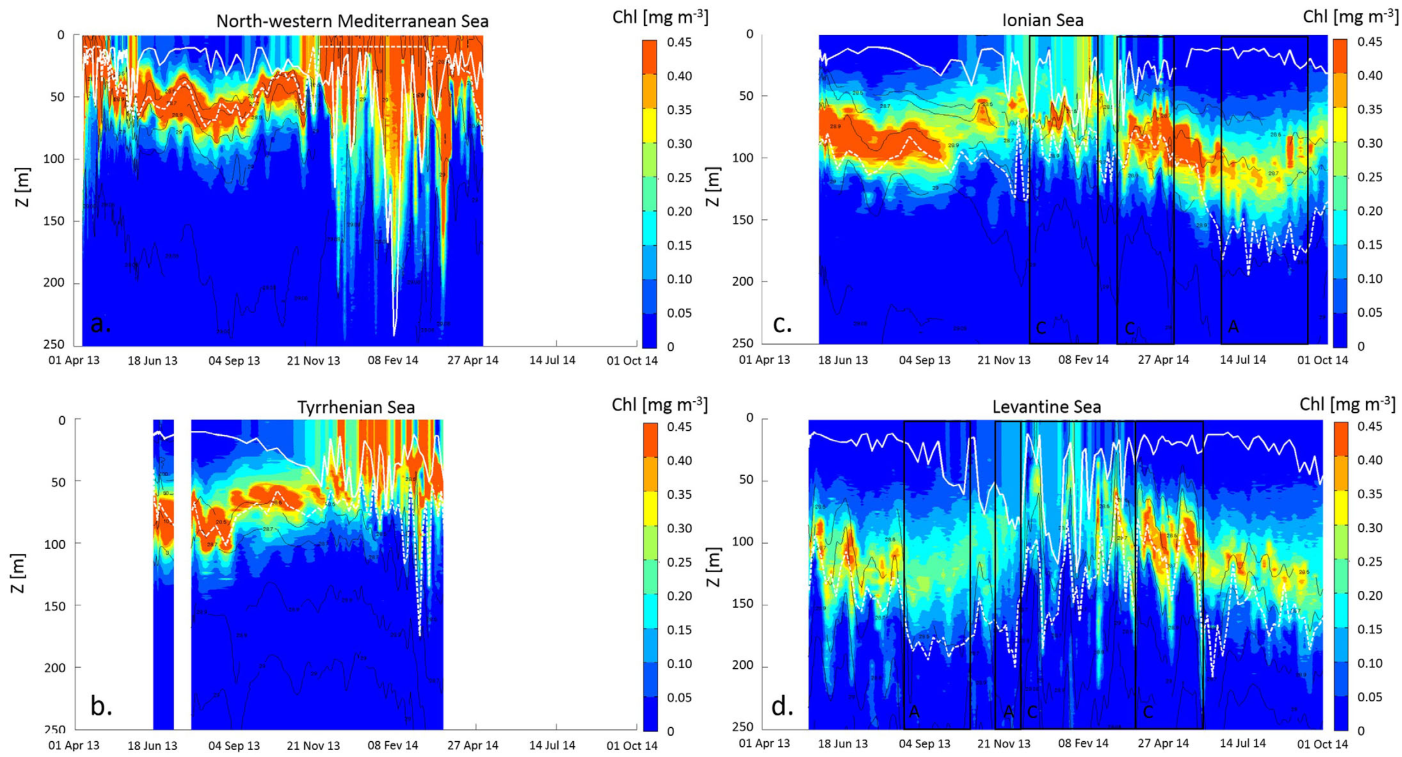


**Figure 12.** [Chl] float transects in (a) the NW Med, (b) TYR, (c) ION, and (d) LEV. Data are interpolated onto a regular grid (1 day × 1 m) with a triangle-based cubic interpolation. Contour plots of density anomalies (28.5 28.7 28.9 29.0 29.06 29.12 29.16, black line), mixed layer depth (solid white line), and nitracline depth (dashed white line) are superimposed. Anticyclonic and cyclonic structures that are discussed in the text are indicated by letters A and C, respectively.

Float data also provide an unrivalled opportunity to track the phytoplankton response to NO3 vertical distribution at short time scale. In the ION and the LEV, our results demonstrate that mesoscale processes do impact on $NO_3$ subsurface distribution, the Chl vertical distribution (and then the DCM) could be likely modulated by mesoscale characteristics. When LEV and ION floats were located in anticyclonic structures (characterized by a deepening of the $Z_{NO3}$), a reduction in subsurface [Chl] was observed, as a consequence of the [$NO_3$] decrease (Figures 12c and 12d, areas indicated by A). For example, in the ION, when the float was entrapped in the anticyclonic structure at the end of the time series, subsurface [Chl] was at its minimum level. Similarly, in the LEV, [Chl] in subsurface sharply decreased from around 0.4 to 0.25 mg $m^{-3}$ in late August 2013, again under anticyclonic conditions. The role of cyclonic structures appears less obvious. An increase in subsurface [Chl] was observed when the $Z_{NO3}$ was close to the surface (e.g., from April to March 2014 in the ION, and from January to May 2014 in the LEV), although not systematically (e.g., from December 2013 to February 2014 in the ION). The data suggest that the potential positive feedback of cyclonic structures on the Chl depends on the relative depths of the different interfaces (i.e., DCM, $Z_{NO3}$, and MLD). Further investigations would be required to clarify this point.

## 6. Conclusion

For the first time in the Med, [$NO_3$] distribution was analyzed using float measurements. This resulted in an unprecedented set of reliable high-frequency [$NO_3$] data that allows the monitoring of a complete annual cycle in four different areas (NW Med, TYR, ION, and LEV).

1. Float data confirm the classical view of the basin, namely the west-to-east decrease of [$NO_3$] and the nitracline deepening and weakening.
2. The nitracline (depth and shape) plays a role at least as important as the MLD in controlling annual cycles.
3. The NW Med is the only area where the MLD exceeds by far the $Z_{NO3}$, and where a significant increase in $[NO_3]_{surf}$ is observed in winter (temperate-like dynamics), with values greater than 6 $\mu M$. In the other

areas, the MLD never crosses the $Z_{NO3}$, and $[NO_3]_{surf}$ is permanently around 0 $\mu M$ (subtropical dynamics).

4. In the NW Med, most of the variability is observed at surface and seasonal physical processes mainly control $[NO_3]$ distribution and $[NO_3]$ seasonal cycle. Conversely, seasonal processes poorly constrain $[NO_3]$ distribution in the other areas (although it is difficult to conclude for the case of TYR) and most of the variability is observed at subsurface.
5. The MLD deepening in the NW Med is characterized by a succession of events that may not be well depicted at climatological scale (i.e., with standard measurements).
6. The frequency and the number of deepening events are key parameters that largely control the quantity of $[NO_3]$ supplied to the photic layer (i.e., usable by primary producers) in the NW Med. Beyond a certain worth, the depth reached by the MLD (classical point of view) is secondary.
7. Mesoscale structures strongly impact the vertical $[NO_3]$ distribution, being furthermore the primary source of variability over the eastern basin.
8. The observed differences in the $NO_3$ seasonal dynamics of the different basins are reflected by different Chl responses. Interactions between [Chl] and $[NO_3]$ fields at shorter time scales are, however, complex and require further measurements and analyses.
9. Therefore, there are limitations in interpreting the data, particularly with respect to phosphate in the eastern basin where the discrepancy between nitracline and phosphacline depth can reach almost 100 m [*Pujo-Pay et al*., 2011].
10. In June 2014, 14 Bio-Argo floats, all equipped with a SUNA sensor, were deployed in the whole Med (second NAOS deployment wave). This data set will allow to confirm or refute some statements of this paper and to go deeper in interannual analysis of the $[NO_3]$ field.

**Acknowledgments**
This paper is a contribution to the French "Equipement d'avenir" NAOS project (ANR J11R107-F). Bio-Argo data used in this work are made available online (http://www.oao.obs-vlfr.fr/BD_FLOAT/NETCDF/). The grant provided by the ACRI-ST company and the French National Association for Research and Technology (ANRT) is also acknowledged. The authors are also grateful to the remOcean project, funded by the European Research Council (grant agreement 246777), and to the French Bio-Argo project funded by CNES-TOSCA. that supported this work. Altimetry-derived maps of Sea Level Anomaly were produced by Ssalto/Duacs and distributed by AVISO, with support from CNES (http://www.aviso.altimetry.fr/duacs). We also thank Kenneth Johnson (Monterey Bay Aquarium Research Institute, USA) for constructive comments and suggestions.

## References


Ascani, F., K. J. Richards, E. Firing, S. Grant, K. S. Johnson, Y. Jia, R. Lukas, and D. M. Karl (2013), Physical and biological controls of nitrate concentrations in the upper subtropical North Pacific Ocean, *Deep Sea Res., Part II*, *93*, 119–134.

Astraldi, M., S. Balopoulos, J. Candela, J. Font, M. Gacic, G. Gasparini, B. Manca, A. Theocharis, and J. Tintoré (1999), The role of straits and channels in understanding the characteristics of Mediterranean circulation, *Prog. Oceanogr.*, *44*(1), 65–108.

Astraldi, M., G. Gasparini, A. Vetrano, and S. Vignudelli (2002), Hydrographic characteristics and interannual variability of water masses in the central Mediterranean: A sensitivity test for long-term changes in the Mediterranean Sea, *Deep Sea Res., Part I*, *49*(4), 661–680.

Bartoli, G., C. Migon, and R. Losno (2005), Atmospheric input of dissolved inorganic phosphorus and silicon to the coastal northwestern Mediterranean Sea: Fluxes, variability and possible impact on phytoplankton dynamics, *Deep Sea Res., Part I*, *52*(11), 2005–2016, doi:10.1016/j.dsr.2005.06.006.

Bates, N. R., A. H. Knap, and A. F. Michaels (1998), Contribution of hurricanes to local and global estimates of air–sea exchange of $CO_2$, *Nature*, *395*(6697), 58–61.

Bosc, E., A. Bricaud, and D. Antoine (2004), Seasonal and interannual variability in algal biomass and primary production in the Mediterranean Sea, as derived from 4 years of SeaWiFS observations, *Global Biogeochem. Cycles*, *18*, GB1005, doi:10.1029/2003GB002034.

Boss, E., M. J. Perry, D. Swift, L. Taylor, P. Brickley, J. R. V. Zaneveld, and S. Riser (2008), Three years of ocean data from a bio-optical profiling float, *Eos Trans. AGU*, *89*(23), 209–210.

Bosse, A., P. Testor, L. Mortier, L. Prieur, V. Taillandier, F. D'Ortenzio, and L. Coppola (2015), Spreading of Levantine Intermediate Waters by submesoscale coherent vortices in the northwestern Mediterranean Sea as observed with gliders, *J. Geophys. Res.: Oceans*, *120*, 1599–1622, doi:10.1002/2014JC010263.

Copin-Montégut, C. (2000), Consumption and production on scales of a few days of inorganic carbon, nitrate and oxygen by the planktonic community: Results of continuous measurements at the Dyfamed Station in the northwestern Mediterranean Sea (May 1995), *Deep Sea Res., Part I*, *47*(3), 447–477.

Coste, B., P. Le Corre, and H. J. Minas (1988), Re-evaluation of the nutrient exchanges in the Strait of Gibraltar, *Deep Sea Res., Part A*, *35*(5), 767–775.

Crise, A., G. Crispi, and E. Mauri (1998), A seasonal three-dimensional study of the nitrogen cycle in the Mediterranean Sea: Part I. Model implementation and numerical results, *J. Mar. Syst.*, *18*(1), 287–312.

Crise, A., J. Allen, J. Baretta, G. Crispi, R. Mosetti, and C. Solidoro (1999), The Mediterranean pelagic ecosystem response to physical forcing, *Prog. Oceanogr.*, *44*(1), 219–243.

Crispi, G., R. Mosetti, C. Solidoro, and A. Crise (2001), Nutrients cycling in Mediterranean basins: The role of the biological pump in the trophic regime, *Ecol. Modell.*, *138*(1), 101–114.

Cullen, J. J. (1982), The deep chlorophyll maximum: Comparing vertical profiles of chlorophyll *a*, *Can. J. Fish. Aquat. Sci.*, *39*(5), 791–803.

Cullen, J. J., P. J. Franks, D. M. Karl, and A. Longhurst (2002), Physical influences on marine ecosystem dynamics, *Sea*, *12*, 297–336.

de Boyer Montégut, C., G. Madec, A. S. Fischer, A. Lazar, and D. Iudicone (2004), Mixed layer depth over the global ocean: An examination of profile data and a profile-based climatology, *J. Geophys. Res.*, *109*, C12003, doi:10.1029/2004JC002378.

D'Ortenzio, F., and M. Ribera d'Alcalà (2009), On the trophic regimes of the Mediterranean Sea: A satellite analysis, *Biogeosciences*, *6*(2), 139–148.

D'Ortenzio, F., M. Ragni, S. Marullo, and M. Ribera d'Alcalà (2003), Did biological activity in the Ionian Sea change after the Eastern Mediterranean Transient? Results from the analysis of remote sensing observations, *J. Geophys. Res.*, *108*(C9), 8113, doi:10.1029/2002JC001556.

D'Ortenzio, F., D. Iudicone, C. de Boyer Montegut, P. Testor, D. Antoine, S. Marullo, R. Santoleri, and G. Madec (2005), Seasonal variability of the mixed layer depth in the Mediterranean Sea as derived from in situ profiles, *Geophys. Res. Lett.*, *32*, L12605, doi:10.1029/2005GL022463.

D'Ortenzio, F., S. Le Reste, H. Lavigne, F. Besson, H. Claustre, L. Coppola, A. Dufour, V. Dutreuil, A. Laes, and E. Leymarie (2012), Autonomously profiling the nitrate concentrations in the ocean: The Pronuts project, *Mercator Ocean Coriolis Q. Newsl.*, *45*, 8–11.

D'Ortenzio, F., H. Lavigne, F. Besson, H. Claustre, L. Coppola, N. Garcia, A. Laës-Huon, S. Le Reste, D. Malardé, and C. Migon (2014), Observing mixed layer depth, nitrate and chlorophyll concentrations in the northwestern Mediterranean: A combined satellite and $NO_3$ profiling floats experiment, *Geophys. Res. Lett.*, *41*, 6443–6451, doi:10.1002/2014GL061020.

Durrieu de Madron, X., C. Guieu, R. Sempéré, P. Conan, D. Cossa, F. D'Ortenzio, C. Estournel, F. Gazeau, C. Rabouille, and L. Stemmann (2011), Marine ecosystems' responses to climatic and anthropogenic forcings in the Mediterranean, *Prog. Oceanogr.*, *91*(2), 97–166.

Durrieu de Madron, X., L. Houpert, P. Puig, A. Sanchez-Vidal, P. Testor, A. Bosse, C. Estournel, S. Somot, F. Bourrin, and M.-N. Bouin (2013), Interaction of dense shelf water cascading and open-sea convection in the northwestern Mediterranean during winter 2012, *Geophys. Res. Lett.*, *40*, 1379–1385, doi:10.1002/grl.50331.

Fernández, V., D. E. Dietrich, R. L. Haney, and J. Tintoré (2005), Mesoscale, seasonal and interannual variability in the Mediterranean Sea using a numerical ocean model, *Progr. Oceanogr.*, *66*(2), 321–340.

Gačić, M., G. Civitarese, S. Miserocchi, V. Cardin, A. Crise, and E. Mauri (2002), The open-ocean convection in the Southern Adriatic: A controlling mechanism of the spring phytoplankton bloom, *Cont. Shelf Res.*, *22*(14), 1897–1908.

Hamad, N., C. Millot, and I. Taupier-Letage (2006), The surface circulation in the eastern basin of the Mediterranean Sea, *Sci. Mar.*, *70*(3), 457–503.

Heimbürger, L.-E., H. Lavigne, C. Migon, F. D'Ortenzio, C. Estournel, L. Coppola, and J.-C. Miquel (2013), Temporal variability of vertical export flux at the DYFAMED time-series station (Northwestern Mediterranean Sea), *Prog. Oceanogr.*, *119*, 59–67.

Henson, S. A., J. P. Dunne, and J. L. Sarmiento (2009), Decadal variability in North Atlantic phytoplankton blooms, *J. Geophys. Res.*, *114*, C04013, doi:10.1029/2008JC005139.

Herrmann, M. J., and S. Somot (2008), Relevance of ERA40 dynamical downscaling for modeling deep convection in the Mediterranean Sea, *Geophys. Res. Lett.*, *35*, L04607, doi:10.1029/2007GL032442.

Hopkins, T. (1988), Recent observations on the intermediate and deep water circulation in the Southern Tyrrhenian Sea, *Oceanol. Acta*, *9*, 41–50.

Houpert, L., P. Testor, X. Durrieu de Madron, S. Somot, F. D'Ortenzio, C. Estournel, and H. Lavigne (2015), Seasonal cycle of the mixed layer, the seasonal thermocline and the upper-ocean heat storage rate in the Mediterranean Sea derived from observations, *Prog. Oceanogr.*, *132*(0), 333–352, doi:10.1016/j.pocean.2014.11.004.

Ignatiades, L., O. Gotsis-Skretas, K. Pagou, and E. Krasakopoulou (2009), Diversification of phytoplankton community structure and related parameters along a large-scale longitudinal east–west transect of the Mediterranean Sea, *J. Plankton Res.*, *31*(4), 411–428.

Isern-Fontanet, J., E. García-Ladona, and J. Font (2003), Identification of marine eddies from altimetric maps, *J. Atmos. Oceanic Technol.*, *20*(5), 772–778.

Jenkins, W., D. McGillicuddy, and D. Lott (2008), The distributions of, and relationship between, $^3$He and nitrate in eddies, *Deep Sea Res., Part II*, *55*(10), 1389–1397.

Johnson, K. S., and L. J. Coletti (2002), In situ ultraviolet spectrophotometry for high resolution and long-term monitoring of nitrate, bromide and bisulfide in the ocean, *Deep Sea Res., Part I*, *49*(7), 1291–1305.

Johnson, K. S., J. A. Needoba, S. C. Riser, and W. J. Showers (2007), Chemical sensor networks for the aquatic environment, *Chem. Rev.*, *107*(2), 623–640.

Johnson, K. S., S. C. Riser, and D. M. Karl (2010), Nitrate supply from deep to near-surface waters of the North Pacific subtropical gyre, *Nature*, *465*(7301), 1062–1065, doi:10.1038/nature09170.

Johnson, K. S., L. J. Coletti, H. W. Jannasch, C. M. Sakamoto, D. D. Swift, and S. C. Riser (2013), Long-term nitrate measurements in the ocean using the In Situ Ultraviolet Spectrophotometer: Sensor integration into the Apex profiling float, *J. Atmos. Oceanic Technol.*, *30*(8), 1854–1866.

Krivosheia, V. G., I. M. Ovchinnikov (1973), Properties of the geostrophic circulation of the Tyrrhenian Sea, *Oceanology*, *13*, 822–827.

Krom, M., S. Brenner, N. Kress, A. Neori, and L. Gordon (1992), Nutrient dynamics and new production in a warm-core eddy from the Eastern Mediterranean Sea, *Deep Sea Res., Part A*, *39*(3), 467–480.

Krom, M., K. Emeis, and P. Van Cappellen (2010), Why is the Eastern Mediterranean phosphorus limited?, *Prog. Oceanogr.*, *85*(3), 236–244.

Larnicol, G., P. Y. Le Traon, N. Ayoub, and P. De Mey (1995), Mean sea level and surface circulation variability of the Mediterranean Sea from 2 years of TOPEX/POSEIDON altimetry, *J. Geophys. Res.*, *100*(C12), 25,163–25,177, doi:10.1029/95JC01961.

Lavezza, R., et al. (2011), Compilation of quality controlled nutrient profiles from the Mediterranean Sea, doi:10.1594/PANGAEA.771907.

Lavigne, H., F. D'Ortenzio, H. Claustre, and A. Poteau (2012), Towards a merged satellite and in situ fluorescence ocean chlorophyll product, *Biogeosciences*, *9*(6), 2111–2125.

Lavigne, H., F. D'Ortenzio, C. Migon, H. Claustre, P. Testor, M. R. d'Alcalà, R. Lavezza, L. Houpert, and L. Prieur (2013), Enhancing the comprehension of mixed layer depth control on the Mediterranean phytoplankton phenology, *J. Geophys. Res. Oceans*, *118*(7), 3416–3430, doi:10.1002/jgrc.20251.

Lavigne, H., F. D'Ortenzio, M. Ribera D'Alcalà, H. Claustre, R. Sauzède, and M. Gacic (2015), On the vertical distribution of the chlorophyll *a* concentration in the Mediterranean Sea: A basin scale and seasonal approach, *Biogeosci. Discuss.*, *12*(5), 4139–4181.

Lazzari, P., C. Solidoro, V. Ibello, S. Salon, A. Teruzzi, K. Béranger, S. Colella, and A. Crise (2012), Seasonal and inter-annual variability of plankton chlorophyll and primary production in the Mediterranean Sea: A modelling approach, *Biogeosciences*, *9*(1), 217–233.

Ledwell, J. R., D. J. McGillicuddy, and L. A. Anderson (2008), Nutrient flux into an intense deep chlorophyll layer in a mode-water eddy, *Deep Sea Res., Part II*, *55*(10), 1139–1160.

Leymarie, E., A. Poteau, X. Andre, F. Besson, P. Brault, H. Claustre, A. David, F. D'Ortenzio, A. Dufour, and H. Lavigne (2013), Development and validation of the new ProvBioII float, *Mercator Ocean Q. Newsl.*, *48*, 26–30.

Longhurst, A., S. Sathyendranath, T. Platt, and C. Caverhill (1995), An estimate of global primary production in the ocean from satellite radiometer data, *J. Plankton Res.*, *17*(6), 1245–1271.

Maillard, C., E. Balopoulos, A. Giorgetti, M. Fichaut, A. Iona, M. Larour, A. Latrouite, B. Manca, G. Maudire, and P. Nicolas (2002), An integrated system for managing multidisciplinary oceanographic data collected in the Mediterranean Sea during the basin-scale research project EU/MAST-MATER (1996–2000), *J. Mar. Syst.*, *33*, 523–538.

Maillard, C., M. Fichaut, G. Maudire, C. Coatanoan, B. Boudjelall, N. Eddalia, J. Beckers, M. Rixen, G. Kortchev, and G. Zodiatis (2005), MEDAR/MEDATLAS 1998–2001: A Mediterranean and Black Sea oceanographic data base and network, *Boll. Geofis. Teor. Appl.*, *46*(4), 329–344.

Manca, B., M. Burca, A. Giorgetti, C. Coatanoan, M.-J. Garcia, and A. Iona (2004), Physical and biochemical averaged vertical profiles in the Mediterranean regions: An important tool to trace the climatology of water masses and to validate incoming data from operational oceanography, *J. Mar. Syst.*, *48*(1), 83–116.
Mann, K., and J. Lazier (2009), *Dynamics of Marine Ecosystems: Biological-Physical Interactions in the Oceans*, John Wiley, Hoboken, N. J.
Marsaleix, P., F. Auclair, J. W. Floor, M. J. Herrmann, C. Estournel, I. Pairaud, and C. Ulses (2008), Energy conservation issues in sigma-coordinate free-surface ocean models, *Ocean Modell.*, *20*(1), 61–89.
Marty, J.-C., J. Chiavérini, M.-D. Pizay, and B. Avril (2002), Seasonal and interannual dynamics of nutrients and phytoplankton pigments in the western Mediterranean Sea at the DYFAMED time-series station (1991–1999), *Deep Sea Res., Part II*, *49*(11), 1965–1985.
McGillicuddy, D., and A. Robinson (1997), Eddy-induced nutrient supply and new production in the Sargasso Sea, *Deep Sea Res., Part I*, *44*(8), 1427–1450.
McGillicuddy, D., A. Robinson, D. Siegel, H. Jannasch, R. Johnson, T. Dickey, J. McNeil, A. Michaels, and A. Knap (1998), Influence of mesoscale eddies on new production in the Sargasso Sea, *Nature*, *394*(6690), 263–266.
McGillicuddy, D. J., L. A. Anderson, N. R. Bates, T. Bibby, K. O. Buesseler, C. A. Carlson, C. S. Davis, C. Ewart, P. G. Falkowski, and S. A. Goldthwait (2007), Eddy/wind interactions stimulate extraordinary mid-ocean plankton blooms, *Science*, *316*(5827), 1021–1026.
Menzel, D. W., and J. H. Ryther (1960), The annual cycle of primary production in the Sargasso Sea off Bermuda, *Deep Sea Res.*, *6*, 351–367.
Migon, C., G. Copin-montegut, L. Elégant, and J. Morelli (1989), Etude de l'apport atmosphérique en sels nutritifs au milieu côtier méditerranéen et implications biogéochimiques, *Oceanol. Acta*, *12*(2), 187–191.
Millot, C. (1991), Mesoscale and seasonal variabilities of the circulation in the western Mediterranean, *Dyn. Atmos. Oceans*, *15*(3), 179–214.
Millot, C., and I. Taupier-Letage (2005), Circulation in the Mediterranean Sea, in Saliot, A. (Ed.), *The Handbook of Environmental Chemistry, Chemistry of the Mediterranean Sea*. pp. 29–66, Springer.
Mkhinini, N., A. L. S. Coimbra, A. Stegner, T. Arsouze, I. Taupier-Letage, and K. Béranger (2014), Long-lived mesoscale eddies in the eastern Mediterranean Sea: Analysis of 20 years of AVISO geostrophic velocities, *J. Geophys. Res. Oceans*, *119*, 8603–8626, doi:10.1002/2014JC010176.
Morrow, R., F. Birol, D. Griffin, and J. Sudre (2004), Divergent pathways of cyclonic and anti-cyclonic ocean eddies, *Geophys. Res. Lett.*, *31*, L24311, doi:10.1029/2004GL020974.
Moutin, T., and L. Prieur (2012), Influence of anticyclonic eddies on the Biogeochemistry from the Oligotrophic to the Ultraoligotrophic Mediterranean (BOUM cruise), *Biogeosciences*, *9*(10), 3827–3855.
Moutin, T., and P. Raimbault (2002), Primary production, carbon export and nutrients availability in western and eastern Mediterranean Sea in early summer 1996 (MINOS cruise), *J. Mar. Syst.*, *33*, 273–288.
Nelson, N. B. (1998), Spatial and Temporal Extent of Sea Surface Temperature Modifications by Hurricanes in the Sargasso Sea during the 1995 Season, *Mon. Weather Rev.*, *126*(5), 1364–1368.
Niewiadomska, K., H. Claustre, L. Prieur, and F. D'Ortenzio (2008), Submesoscale physical-biogeochemical coupling across the Ligurian current (northwestern Mediterranean) using a bio-optical glider, *Limnol. Oceanogr.*, *53(5)*, 2210–2225.
Ogura, N., and T. Hanya (1966), Nature of ultra-violet absorption of sea water, *Nature*, *212*, 758, doi:10.1038/212758a0.
Omand, M. M., and A. Mahadevan (2013), Large-scale alignment of oceanic nitrate and density, *J. Geophys. Res. Oceans*, *118*, 5322–5332, doi:10.1002/jgrc.20379.
Omand, M. M., and A. Mahadevan (2015), The shape of the oceanic nitracline, *Biogeosciences*, *12*(11), 3273–3287, doi:10.5194/bg-12-3273-2015.
Pasquero, C., A. Bracco, and A. Provenzale (2005), Impact of the spatiotemporal variability of the nutrient flux on primary productivity in the ocean, *J. Geophys. Res.*, *110*, [10.1029/2004JC002738]
Pasqueron de Fommervault, O., C. Migon, M. R. d'Alcalà, and L. Coppola (2015a), Temporal variability of nutrient concentrations in the northwestern Mediterranean Sea (DYFAMED time-series station), *Deep Sea Res., Part I*, *100*, 1–12.
Pasqueron de Fommervault, O., C. Migon, A. Dufour, F. D'ortenzio, F. Kessouri, P. Raimbault, N. Garcia, and V. Lagadec (2015b), Atmospheric input of inorganic nitrogen and phosphorus to the Ligurian SEA: Data from the cap Ferrat coastal time-series station, *Deep Sea Res., Part I*, *106*, 116–125.
Pujo-Pay, M., P. Conan, L. Oriol, V. Cornet-Barthaux, C. Falco, J. F. Ghiglione, C. Goyet, T. Moutin, and L. Prieur (2011), Integrated survey of elemental stoichiometry (C, N, P) from the western to eastern Mediterranean Sea, *Biogeosciences*, *8*(4), 883–899, doi:10.5194/bg-8-883-2011.
Redfield, A. C. (1934), *On the Proportions of Organic Derivatives in Sea Water and Their Relation to the Composition of Plankton*, in edited by R. J. Daniel, James Johnstone Memorial Volume, pp.177–192, Univ. Press of Liverpool, Liverpool.
Ribera d'Alcalà, M., G. Civitarese, F. Conversano, and R. Lavezza (2003), Nutrient ratios and fluxes hint at overlooked processes in the Mediterranean Sea, *J. Geophys. Res.*, *108*(C9), 8106, doi:10.1029/2002JC001650.
Ribera d'Alcalà, M., C. Brunet, F. Conversano, F. Corato, and R. Lavezza (2009), Nutrient and pigment distributions in the southern Tyrrhenian Sea during mid-summer and late fall 2005, *Deep Sea Res., Part II*, *56*(11), 676–686.
Rinaldi, E., B. Buongiorno Nardelli, E. Zambianchi, R. Santoleri, and P. M. Poulain (2010), Lagrangian and Eulerian observations of the surface circulation in the Tyrrhenian Sea, *J. Geophys. Res.*, *115*, C04024, doi:10.1029/2009JC005535.
Robinson, A., M. Golnaraghi, W. Leslie, A. Artegiani, A. Hecht, E. Lazzoni, A. Michelato, E. Sansone, A. Theocharis, and Ü. Ünlüata (1991), The eastern Mediterranean general circulation: features, structure and variability, *Dyn. Atmos. Oceans*, *15*(3), 215–240.
Robinson, A. R., W. G. Leslie, A. Theocharis, and A. Lascaratos (2001), Mediterranean Sea circulation, in *Ocean Currents: A Derivative of the Encyclopedia of Ocean Sciences*, in Encyclopedia of Ocean Sciences, edited by K. K. Turekian and S. A. Thorpe, pp. 1689–1706, Academic Press, London, U. K.
Ruiz, S., L. Renault, B. Garau, and J. Tintoré (2012), Underwater glider observations and modeling of an abrupt mixing event in the upper ocean, *Geophys. Res. Lett.*, *39*, L01603, doi:10.1029/2011GL050078.
Sakamoto, C. M., K. S. Johnson, and L. J. Coletti (2009), Improved algorithm for the computation of nitrate concentrations in seawater using an in situ ultraviolet spectrophotometer, *Limnol. Oceanogr. Methods*, *7*, 132–143.
Schmechtig, C., C. Claustre, H. Claustre, A. Poteau, and F. D'Ortenzio (2014), Bio-Argo quality control manual for the Chlorophyll-A concentration, report, Ifremer, doi:10.13155/35385. [Available at(http://archimer.ifremer.fr/doc/00243/35385/34456.pdf.]
Severin, T., P. Conan, X. D. de Madron, L. Houpert, M. Oliver, L. Oriol, J. Caparros, J. Ghiglione, and M. Pujo-Pay (2014), Impact of open-ocean convection on nutrients, phytoplankton biomass and activity, *Deep Sea Res., Part I*, *94*, 62–71.
Siokou-Frangou, I., U. Christaki, M. Mazzocchi, M. Montresor, M. Ribera d'Alcalá, D. Vaqué, and A. Zingone (2010), Plankton in the open Mediterranean Sea: A review, *Biogeosciences*, *7*(5), 1543–1586.

Smith, R. O., H. Bryden, and K. Stansfield (2008), Observations of new western Mediterranean deep water formation using Argo floats 2004–2006, *Ocean Sci.*, *4*(2), 133–149.

Steinberg, D. K., C. A. Carlson, N. R. Bates, R. J. Johnson, A. F. Michaels, and A. H. Knap (2001), Overview of the US JGOFS Bermuda Atlantic Time-series Study (BATS): A decade-scale look at ocean biology and biogeochemistry, *Deep Sea Res., Part II*, *48*(8), 1405–1447.

Strickland, J. D., R. Eppley, and B. R. De Mendiola (1969), Phytoplankton populations, nutrients and photosynthesis in Peruvian coastal waters, *Bol. Inst. Mar. Peru*, *2*, 4–45.

Sverdrup, H. U., M. W. Johnson, and R. H. Fleming (1942), *The Oceans: Their Physics, Chemistry, and General Biology*, Prentice Hall, N. Y.

Taupier-Letage, I. (2008), On the use of thermal images for circulation studies: Applications to the Eastern Mediterranean basin, in *Remote Sensing of the European Seas*, edited by V. Barale, and M. Gade, pp. 153–164, Springer.

Tusseau-Vuillemin, M. H., L. Mortier, and C. Herbaut (1998), Modeling nitrate fluxes in an open coastal environment (Gulf of Lions): Transport versus biogeochemical processes, *J. Geophys. Res.*, *103*(C4), 7693–7708.

Van Wambeke, F., J.-F. Ghiglione, J. Nedoma, G. Mével, and P. Raimbault (2009), Short scale variations in nutrients, ectoenzymatic activities and bottom-up effects on bacterial production and community structure during late summer-autumn transition in the open NW Mediterranean Sea, *Biogeosci. Discuss.*, *6*, 687–727.

Violaki, K., J. Sciare, J. Williams, A. Baker, M. Martino, and N. Mihalopoulos (2015), Atmospheric water-soluble organic nitrogen (WSON) over marine environments: A global perspective, *Biogeosciences*, *12*(10), 3131–3140.

While, J., and K. Haines (2010), A comparison of the variability of biological nutrients against depth and potential density, *Biogeosciences*, *7*(4), 1263–1269.

Wong, A., R. Keeley, and T. Carval (2014), Argo Quality Control Manual, Version 3.0, doi:10.13155/33951. [Available at http://archimer.ifremer.fr/doc/00228/33951/32470.pdf.]

Xing, X., A. Morel, H. Claustre, D. Antoine, F. D'Ortenzio, A. Poteau, and A. Mignot (2011), Combined processing and mutual interpretation of radiometry and fluorimetry from autonomous profiling Bio-Argo floats: Chlorophyll *a* retrieval, *J. Geophys. Res.*, *116*, C06020, doi:10.1029/2010JC006899.